GLIA

WILEY

RESEARCH ARTICLE

Astrocytic p75^{NTR} expression provoked by ischemic stroke exacerbates the blood–brain barrier disruption

Xiaoying Qin[1] | Jianing Wang[1] | Shujian Chen[1] | Gang Liu[1] |
Chaoran Wu[1] | Qunyu Lv[1] | Xinran He[1] | Xianshu Bai[2] |
Wenhui Huang[2] | Hong Liao[1]

[1]New drug screening center, Jiangsu Center for Pharmacodynamics Research and Evaluation, China Pharmaceutical University, Nanjing, China

[2]Molecular Physiology, Center for Integrative Physiology and Molecular Medicine (CIPMM), University of Saarland, Homburg, Germany

Correspondence
Hong Liao, New drug screening center, Jiangsu Center for Pharmacodynamics Research and Evaluation, China Pharmaceutical University, 24 Tongjiaxiang, 210009 Nanjing, China.
Email: hliao@cpu.edu.cn
Wenhui Huang, Molecular Physiology, Center for Integrative Physiology and Molecular Medicine (CIPMM), University of Saarland, 66421 Homburg, Germany.
Email: wenhui.huang@uks.eu

Abstract

The disruption of the blood–brain barrier (BBB) plays a critical role in the pathology of ischemic stroke. p75 neurotrophin receptor (p75^{NTR}) contributes to the disruption of the blood-retinal barrier in retinal ischemia. However, whether p75^{NTR} influences the BBB permeability after acute cerebral ischemia remains unknown. The present study investigated the role and underlying mechanism of p75^{NTR} on BBB integrity in an ischemic stroke mouse model, middle cerebral artery occlusion (MCAO). After 24 h of MCAO, astrocytes and endothelial cells in the infarct-affected brain area up-regulated p75^{NTR}. Genetic p75^{NTR} knockdown (p75^{NTR+/−}) or pharmacological inhibition of p75^{NTR} using LM11A-31, a selective inhibitor of p75^{NTR}, both attenuated brain damage and BBB leakage in MCAO mice. Astrocyte-specific conditional knockdown of p75^{NTR} mediated with an adeno-associated virus significantly ameliorated BBB disruption and brain tissue damage, as well as the neurological functions after stroke. Further molecular biological examinations indicated that astrocytic p75^{NTR} activated NF-κB and HIF-1α signals, which upregulated the expression of MMP-9 and vascular endothelial growth factor (VEGF), subsequently leading to tight junction degradation after ischemia. As a result, increased leukocyte infiltration and microglia activation exacerbated brain injury after stroke. Overall, our results provide novel insight into the role of astrocytic p75^{NTR} in BBB disruption after acute cerebral ischemia. The p75^{NTR} may therefore be a potential therapeutic target for the treatment of ischemic stroke.

KEYWORDS
astrocyte, blood–brain barrier, ischemic stroke, p75^{NTR}, tight junction proteins

1 | INTRODUCTION

Ischemic stroke is a leading cause of mortality and long-term disability worldwide (Matsumoto et al., 2020). It constitutes a major public health burden, yet current therapeutic interventions are limited (Pirson et al., 2020). Thus, there is an urgent need for investigating the mechanism of stroke-induced ischemic injury to find potential pharmacological targets of the disease.

Blood–brain barrier (BBB) breakdown is a hallmark of ischemic stroke, which contributes to the brain pathology (Abdullahi et al., 2018;

Kassner & Merali, 2015).Therefore, protecting the BBB may be a therapeutic strategy for alleviating brain ischemia injury. The BBB is composed of endothelial cells lining the cerebral vasculature, pericytes, and astrocytic end-feet. The static barrier function of the BBB mainly dependents on endothelial cells and the tight junctions, which restricts paracellular permeability. BBB disruption leads to vasogenic edema, hemorrhagic transformation, and leukocyte infiltration, thereby augmenting cerebral inflammation and total ischemic brain damage (Bernstein et al., 2020; Wang et al., 2020). Previous studies reported various mechanisms leading to BBB breakdown after stroke, including endothelial dysfunction with abnormal structural alternations of tight junctions (Jiang et al., 2018; Knowland et al., 2014; Krueger et al., 2019), and activation of matrix metalloproteinases (MMPs) causing degradation of endothelial tight junctions (Prakash & Carmichael, 2015; Zhang, Tang, et al., 2020), and so forth.

Ischemic injury also triggers tremendous activation of glial cells (Huang et al., 2020; Morizawa et al., 2017; Patabendige et al., 2021; Williamson et al., 2021). Emerging evidence suggests key roles of astrocytes in BBB breakdown after cerebral ischemia (Begum et al., 2018; Michinaga & Koyama, 2019). On one hand, ion channels (especially the Kir4.1 potassium channel) and the water channel proteins (especially aquaporin 4, AQP4) expressed on the astrocytic end-feet directly regulate ions and water balance, the increase of which causes swelling of astrocytic end-feet and further exacerbats brain edema and BBB disruption after stroke (Filchenko et al., 2020; Vella et al., 2015). On the other hand, activated astrocytes release chemical molecules (e.g., nitric oxide and glutamate) and proteins (e.g., MMPs, vascular endothelial growth factors [VEGF], and endothelin-1), to disrupt endothelial TJs, enhancing BBB breakdown after ischemic injury (András et al., 2007; Li et al., 2014; Lo et al., 2005; Saha & Pahan, 2006; Yang et al., 2019; Zhang et al., 2018). Particularly, MMPs (such as MMP9) cause degradation of tight junction proteins (claudin-5 and occludin, OCLN) and extracellular matrix molecules (including collagen, laminin, and fibronectin) while VEGF interacts with the receptor tyrosine kinases (VEGFR) on endothelial cells to downregulate TJ protein expression, accelerating BBB leakage in the acute phase of stroke (Chen et al., 2019; Wu et al., 2018; Yang et al., 2007). However, astrocytes were also reported to play certain protective roles during ischemic stroke. For example, astrocytes not only provide energy support (Hayakawa et al., 2016), but also produce a variety of proteins such as angiopoietin-1, Sonic Hedgehog, apolipoprotein E (ApoE) and various growth factors (e.g., Glial cell-derived neurotrophic factor, GDNF and insulin-like growth factor-1, IGF-1) to inhibit brain endothelial apoptosis, promote endothelial proliferation and enhance expression and reassembly of tight junction proteins (claudin-5, OCLN, and ZO-1), ameliorating the recovery of the BBB (Bake et al., 2019; Liu et al., 2022; Xia et al., 2013). Taken together, the role (and its underlying mechanisms) of astrocytes in regulating BBB functions during cerebral ischemia remains elusive.

The p75 neurotrophin receptor (p75^{NTR}), also called nerve growth factor receptor (NGFR), is a member of the TNF receptor super family (Schachtrup et al., 2015). While its expression is very low in healthy adult brain tissues, it is dramatically upregulated upon various pathological insults, for example, traumatic brain injury (Schachtrup et al., 2015;

Shi et al., 2013), amyotrophic lateral sclerosis (Taylor et al., 2012), Alzheimer's disease (Mufson et al., 2019; Nguyen et al., 2014), and ischemic stroke (Irmady et al., 2014; Jover et al., 2002; Oderfeld-Nowak et al., 2003; Park et al., 2000). In a MCAO (middle cerebral artery occlusion)-induced ischemic stroke model, the infarct volume of p75$^{NTR-/-}$ mice was significantly reduced compared with the wildtype (WT) mice, suggesting a deleterious role of p75^{NTR} in ischemia (Irmady et al., 2014). Indeed, the p75^{NTR} was found to induce neuronal apoptosis and degeneration under pathological conditions such as ischemia (Irmady et al., 2014; Jover et al., 2002; Nguyen et al., 2014; Taylor et al., 2012). In addition to neurons, previous studies demonstrated that p75^{NTR} expression was also increased in astrocytes after ischemic stroke, though its function is unclear (Oderfeld-Nowak et al., 2003). Notably, the expression of p75^{NTR} was found to be increased in Müller glia in the retina in several disease models (e.g., oxygen-induced retinopathy) (Barcelona et al., 2016; Elshaer et al., 2019; Lebrun-Julien et al., 2010; Mysona et al., 2013). Further studies revealed that such upregulated p75^{NTR} induced the inflammatory cytokine production by Müller glia, which promoted the blood-retina barrier disruption during retinal ischemia (Barcelona et al., 2016; Mysona et al., 2013), suggesting astrocytic p75^{NTR} in the brain may also play important roles in regulating BBB function in cerebral ischemic stroke.

In the current study we focused on the effect and potential molecular mechanisms of astrocytic p75^{NTR} regulating BBB integrity after ischemic stroke. We reported that p75^{NTR} expression was significantly increased in astrocytes and endothelial cells in and around the infarct area of mouse brain after cerebral ischemia. Both genetic knockdown of p75^{NTR} (p75$^{NTR+/-}$) and adeno-associated virus (AAV) mediated astrocyte-specific p75^{NTR} conditional knockdown (cKD) significantly ameliorated the brain tissue damage and BBB leakage. The mechanisms of astrocytic p75^{NTR} causing BBB disruption involved activation of NF-κB and HIF-1α signals, which upregulated MMP-9 and VEGF, thus leading to degradation of tight junction proteins. LM11A-31, an inhibitor of p75^{NTR}, also exhibited a protective effect on ischemic brain injury. Taken together, our results provided novel insight into the role of astrocytic p75^{NTR} in BBB breakdown and p75^{NTR} might be a potential therapeutic target for the treatment of ischemic stroke.

2 | MATERIALS AND METHODS

2.1 | Experimental animals

All experimental protocols and animal handling procedures were approved by the Animal Research Ethics Committee of China Pharmaceutical University (Approval No.: 2020–12–002) and were performed in accordance with institutional, national and international guidelines for animal care and welfare. The breeding pairs of p75^{NTR} knockout mice (p75^{NTR}/ExonIII$^{-/-}$, p75$^{NTR-/-}$) on a B6.129S background were given by Professor Yanjiang Wang from the Third Military Medical University as a gift; and GFAP-cre transgenic mice on a B6.Cg background were purchased from the Jaxson Laboratory (ME, USA; #024098). Wild type C57BL/6J mice were purchased from Vital River Laboratory

Animal Technology (Beijing, China). All the animals were raised and bred under specific pathogen-free conditions in the Animal Research Centre of China Pharmaceutical University. Mutants were outbred for more than six generations to obtain p75^{NTR} heterozygotes and GFAP-cre transgenic mice used in this study. All mice were kept on a standard 12 h light-to-dark cycle with ad libitum access to food and water.

2.2 | Transient middle cerebral artery occlusion

A transient right MCAO was performed as previously described (Zhang, Tang, et al., 2020). Briefly, 10–12-week-old male mice were anesthetized with 1.5% isoflurane using a Rodent Anesthesia Machine (RWD Life Science, Shenzhen, China). Then, the right common carotid artery, internal carotid artery (ICA), and external carotid artery (ECA) were surgically exposed. A silicone-coated surgical nylon filament (Sunbio Biotech, Beijing, China) was inserted into the right ICA through the ECA stump to block the origin of the middle cerebral artery, when a slight resistance was felt, the threading was stopped. The filament was placed there for 1 h, resulting in ischemic injury. One hour later, the filament was gently removed for the reperfusion. The mice of the sham group underwent the same procedures except for filament insertion. Warming pads were used to maintain the rectal temperatures at 37.0 ± 0.5°C during surgery. Mice in which regional cerebral blood flow did not reduced at least 75% of baseline (Figure S1a) according to laser Doppler flowmetry (Perimed, Hong Kong, China) were excluded from the study. We also observed stroke outcomes induced by the MCAO surgery. The cerebral infarction reached 47.33 ± 9.14% and neurological functional deficits occurred (measured by neurological severity scores [NSS]) (Figure S1).

2.3 | Adeno-associated virus injection

Adeno-associated virus (generic serotype 2/9 AAV) of p75^{NTR} and the control AAV were purchased from Hanbio Biotechnology (Shanghai, China). To knockdown p75^{NTR}, we designed a siRNA oligomer targeting the mouse _Ngfr_ (5′-GGTCGAGAAGCTGCTCAAT-3′). This siRNA was cloned into a Cre-dependent and miR30-based shRNA expression vector (pAKD-CMV-bGlobin-FLEX-miR30-sh-p75^{NTR}), which was packed into AAV (generic serotype 2/9). The AAV9 (pAKD-CMV-bGlobin-FLEX) was used as control. To allow the expression of miR30-sh-p75^{NTR} in astrocytes, we injected the designed AAV into the brain of GFAP-Cre mice. Briefly, 21 days before MCAO, the male mice were anesthetized with 1.5% isoflurane before AAV injection (RWD Life Science, Shenzhen, China). One microliter (1 × 10^{13} units/μl) of AAV was injected into the right cerebral cortices of GFAP-cre mice using a stereotaxic apparatus (RWD Life Science, Shenzhen, China) according to a previous report (Caracciolo et al., 2018). The stereotaxic coordinates of the injection location were as follows: 0.2 mm anterior, 0.75 mm ventral, and 1.5 mm right lateral to the bregma. The temperature of mice was maintained at 37.5 ± 0.5°C during the operation by using a heating pad till the mice were fully awake from the anesthetized state.

2.4 | Neurological function assessment

Neurological functions were evaluated at 24 h after reperfusion according to the guidelines of the NSS (Flierl et al., 2009). The whole assessment was performed by an investigator who was blinded to the groupings. The scale was based on the following eight individual tests: (1) Exit circle; (2) Seeking behavior; (3) Monoparesis/ hemiparesis; (4) Straight walk; (5) Startle reflex; (6) Beam balancing; (7) Beam walk; (8) Round stick balancing. The absence of neurological deficits was scored as 0; neurological deficits were scored as 1, except Beam walk test was 0–3 points. The eight individual test scores were summed up at the end of the evaluation (minimum score, 0; maximum score, 10).

2.5 | Measurement of infarct volume and brain edema

At 24 h after reperfusion, mice were sacrificed and the brains were rapidly removed and mildly frozen at −20°C for 10 min (Lin et al., 2013). Infarct volume was then measured by 2,3,5-triphenyltetrazolium chloride (TTC) staining (Peng et al., 2020). Briefly, brains were sliced into five serial 2 mm coronal sections and incubated with 2% TTC solution (Sigma-Aldrich, St. Louis, MO, USA) for 30 min at 37°C in the dark. After fixed with 4% paraformaldehyde solution for 20 min, the images of brain sections were captured using a digital camera and analyzed using ImageJ (http://rsb.info.nih.gov/ij/). To compensate for the effect of brain edema, the corrected infarct volume was calculated as follows: percentage of corrected infarct volume = {[Total lesion volume (TTC negative region) − (ipsilateral hemisphere volume − contralateral hemisphere volume)]/contralateral hemisphere volume} × 100%. Brain edema was evaluated by the enlargement of the ischemic hemisphere as previously described (Liang et al., 2020). Brain edema volume was quantified as: [(ipsilateral hemisphere volume − contralateral hemisphere volume)/contralateral hemisphere volume] × 100%.

2.6 | Evans blue assay

The impaired BBB integrity was measured by Evans Blue (EB) leakage in the brain as previously reported (Wang et al., 2020). EB dye (2%, 4 ml/kg; Sigma-Aldrich) was intravenously administered via the tail vein 23 h after reperfusion. After 1 h of circulation, the mice were anesthetized and perfused with saline. The brains were isolated and cut into five 2-mm-thick coronal slices, which were photographed to visualize the dye leakage. Then, quantitative assessment of the dye content in the ischemic hemispheric tissue was conducted. Ipsilateral brain tissues were weighed and homogenized in 1 ml 50% trichloroacetic acid. After centrifugation (10,000 × _g_, 20 min), the supernatant was collected and measured on a microplate fluorescence reader at 620 nm. The amount of EB dye was expressed as μg/g of wet tissue weight, using a standard curve.

2.7 | Western blot analysis

Total proteins were extracted using RIPA buffer (Beyotime Biotechnology, Haimen, China) with PMSF (Beyotime Biotechnology). The protein concentrations were measured using a BCA protein assay kit (Beyotime Biotechnology). Next, 30 μg per lane proteins were separated by SDS-PAGE and then transferred to nitrocellulose membranes (Millipore, Billerica, MA, USA). The membranes were blocked with 5% non-fat milk in Tris-buffered saline containing 1/1000 Tween 20 for 1 h, then washed twice and probed with primary antibodies overnight at 4°C. The primary antibodies: anti-p75[NTR] (Santa Cruz Biotechnology, Fort Worth, TX, sc-13,577), anti-VEGF (Santa Cruz Biotechnology; sc-7269), anti-OCLN (Invitrogen, Carlsbad, CA; 71–1500), anti-ZO-1 (Invitrogen; 61–7300), anti-AQP4 (Proteintech Group, Rosemount, IL; 16,473-1-AP), anti-MMP9 (Proteintech Group; 10,375-2-AP) and anti-β-actin (Proteintech Group; 20,536-1-AP) were used at 1:1000 dilution. The membranes were washed three times (10 min each) and then incubated with horseradish peroxidase-conjugated goat anti-rabbit/mouse IgG (Sigma-Aldrich) secondary antibodies for 1 h. After rinsing with TBST for three times, the bands were visualized by enhanced chemiluminescence (ECL) Advance Kit (Bio-Rad, Hercules, CA, USA) and quantified by densitometric analysis (ImageJ) (http://rsb.info.nih.gov/ij/). β-actin was used as an internal loading control.

2.8 | Immunofluorescence

Mice were euthanized and sacrificed at 24 h after reperfusion. The brains were perfused with saline followed by fixation with a 4% paraformaldehyde solution, then immersed in 20% and 30% sucrose for 3 days for dehydration. After freezing in a cryostat microtome (SM2000R; Leica, Wetzlar, Germany), the brains were sliced into 20 μm thick sections at the position of bregma approximating −1 to 1 mm using a cryostat (Leica, Buffalo Grove, IL, USA). The sections were permeabilized with 0.3% Triton X-100 in phosphate-buffered saline (PBS) for 15 min. After blocking with 10% goat serum in PBS for 1 h, the sections were incubated with the indicated primary antibodies at 4°C overnight. The primary antibodies were as follows: mouse anti-GFAP (1:500; Millipore Sigma; MAB360), rabbit anti-p75[NTR] (1:300; Promega Corporation, Madison, WI; G3231; Cheng et al., 2018), rat anti-CD31 (1:300; Abcam, Boston, MA; ab56299), rabbit anti-OCLN (1:100; Invitrogen; 71–1500), rabbit anti-ZO-1 (1:50; Invitrogen; 61–7300), rabbit anti-CD45 (1:100; Proteintech Group; 20,103-1-AP), rat anti-CD11b (1:250; eBioscience, San Diego, CA, 14–0112), rabbit anti-Iba1 (1:250; Waco, Wakayama, Japan; 019–19,741) or rat anti-CD68 (1:250; Bio-Rad, Hercules, CA, MCA1957) at 4°C overnight. After rinsing three times, the sections were treated with a mix of the appropriate secondary antibodies—Alexa-Fluor 488/633 conjugated anti-rabbit/mouse or Alexa-Fluor 488/633 conjugated anti-rabbit/rat (1:500; Invitrogen) for 1 h, followed by a 10 min incubation with Hoechst.

Since the ipsilateral dorsal cortex is the most affected area in the MCAO model, we thereby focused on the infarct core and penumbra area in the dorsal cortex. The fluorescent images of the ipsilateral cerebral cortices were captured by an Olympus Fluoview FV1000 confocal microscope (20× objective, Olympus, Japan) from at least four slices per mouse using FV10-ASW 2.0 software. The filter DM405/488/543/633 was used. Specifically, the IF staining images were collected under fixed excitation light intensity and exposure time. For each slide from a mouse, at least five random fields were collected under appropriate magnification. Then, the original images were subjected to average grayscale value on the selected region by using ImageJ software (http://rsb.info.nih.gov/ij/). For mean fluorescence intensity (MFI), a region of interest (ROI) on each image was drawn and add to the ROI manager, the mean gray value of the region was measured. The MFI of ZO-1$^+$ or OCLN$^+$ was normalized by the MFI of CD31$^+$ signals on the same brain region to present the relative MFI.

2.9 | Gelatin zymography assay

Gelatin zymography assay was performed using the MMP Zymography Assay Kit (Shanghai Xinfan biotechnology, Shanghai, China) following the manufacturer's instructions. Brain tissues were homogenized in 0.25% Nacl and the protein concentrations were measured using a BCA protein assay kit (Beyotime Biotechnology). Next, 100 μg per lane proteins were mixed with 2× Non-Reducing Loading buffer and then separated by SDS-PAGE electrophoresis with 8% separating gel containing 10% gelatin. Zymograms were renatured and developed with zinc-containing Reaction Buffer at 37°C for 36 h. After the enzymatic reaction, the gels were stained with Coomassie Brilliant Blue and incubated in destaining solution for 2 h to de-stain. Protease activity seemed as clear bands were quantified by densitometric analysis (ImageJ) (http://rsb.info.nih.gov/ij/).

2.10 | Magnetic-activated cell sorting

Magnetic-activated cell sorting (MAC-sorting) was performed according to previous report (Holt, Stoyanof & Olsen, 2019). At 24 h after MCAO reperfusion, the MCAO mice and the sham operated control mice were perfused with saline (4°C) and the brains were isolated in ice cold D-Hanks buffer. Cortices were dissected from the brains and the ischemic brain tissue in the ipsilateral cerebral cortices was collected and digested with 2 mg/ml papain (MedChem Express, Monmouth Junction, NJ, USA) with 1000 U/ml DNase (Roche Life Science, Penzberg, Germany). The tissue/papain mixture was incubated in a water bath set to 37°C for 30 min. The tubes were swirled every 5 min to maximize the tissue's exposure to the papain. The tissue was gently titrated until the solution was homogenous and centrifuged at 300 × g for 3 min at room temperature. The cell pellet was resuspended in 0.5% BSA in PBS solution. A discontinuous density

gradient was prepared by percoll dissociation solution (a mixture of 1.8 ml percoll, 200 μl 10x D-Hanks, and 8 ml 1x D-Hanks). The cell suspension was carefully layered on top of the percoll dissociation solution and centrifuged at $500 \times g$ for 20 min at room temperature. The pelleted cells were suspended in 0.5% BSA in PBS solution and filtered with a 70 μm BD Falcon filter to remove any non-dissociated tissue and to obtain a single-cell suspension. Then, magnetic cell sorting was conducted according to the manufacturer's instructions using Anti-GLAST MicroBead Kit (Miltenyi Biotec, Germany). Cells were then fluorescently stained with Anti-GLAST (ACSA-1)-PE (Miltenyi Biotec, Germany) and the purity of the sorted astrocytes was ~90% analyzed by flow cytometry (Figure S4b).

2.11 | Astrocyte primary cultures

Astrocyte primary cultures were prepared as previously described (Shan et al., 2019). Briefly, primary cultures of cortical astrocytes were prepared from neonatal C57BL/6 mice at postnatal day 1. Cortices were dissected from the brains, and the meninges were carefully removed. The cortices were dissociated into a cell suspension by digestion with 0.25% trypsin and 1000 U/ml DNase (Roche Life Science) for 10 min at 37°C. After centrifuged at 1500 rpm for 10 min at 4°C, the pellet was resuspended in DMEM/F12 (DF12) medium with 10% FBS and filtered with a 70 μm cell strainer (BD Biosciences, San Jose, CA, USA). The cells were then seeded in 75 cm^2 cell culture flasks at a density of 2.0×10^7 cells/well and cultured at 37°C in a humidified atmosphere of 5% CO2 /95% air. After 7–9 days of culture, the cells reached 80%–90% confluency and were shaken (200 rpm) for 18 h to minimize microglial contamination. Adherent astrocytes were detached and resuspended by using 0.25% trypsin/EDTA (Beyotime Biotechnology), and the recovered cells were cultured on the bottom of a six-well or 24-well plate. Astrocyte purity was determined using immunofluorescence staining for GFAP. Ninety-five percent of the cultured cells were identified as astrocytes.

2.12 | bEnd.3 cell culture

The mouse brain endothelial cell line, bEnd.3, was obtained from the American Type Culture Collection (Manassas, VA, USA) and cultured in DF12 medium (Gibco, Carlsbad, CA, USA) supplemented with 10% FBS (Gibco) and 100 U penicillin/100 μg streptomycin (Invitrogen). The cell medium was refreshed every 2 days, and the cells were subcultured using 0.25% trypsin at a ratio of 1:3 every 3 days (Shan et al., 2019). The bEnd.3 cells used in the experiments were from the 3rd–5th passages.

2.13 | Transfection with siRNA

Small interfering RNA (siRNA) transfection was performed using Lipofectamine 3000 and Opti-MEM following the manufacturer's

instructions (Invitrogen). siRNA that specifically targeted nucleotides 325–343 of mouse p75^{NTR} (GenBank accession no. NM_002507.4) and the scrambled control were purchased from OBiO Technology Corp., Ltd. (Shanghai, China). The sequence of siRNA primers of p75^{NTR} were 5′-CCAACCAGACCGUGUGUGAUU-3′ and 5′-UCAC ACACGGUCUGGUUGGUU-3′. Primary astrocytes were seeded on six-well or 24-well plates the day before transfection. The cells were transfected with p75^{NTR} siRNA or scrambled control (100 nM final concentrations) by 4 μl/ml Lipofectamine 3000 for 6 h. The medium was then replaced with complete DF12 medium. The transfection efficiency was verified 48 h after transfection using fluorescence microscopy.

2.14 | Transfection with p75^{NTR} overexpression lentivirus

The p75^{NTR} overexpression lentivirus and GFP control lentivirus were purchased from OBiO Technology Corp., Ltd. (Shanghai, China) and transfected astrocytes following the manufacturer's instructions. Primary astrocytes were seeded on 24-well plates the day before transfection. The cells were transfected with lentivirus (MOI = 10) with 50 μg/ml (final concentration) polybreme for 24 h. After 24 h transfection, the lentivirus was removed and replaced with complete DF12 medium.

2.15 | Construction of the in vitro BBB model

The in vitro BBB model was constructed as previously described (Ma et al., 2020; Zhang, Tang, et al., 2020). Briefly, astrocytes were plated on the bottom of a 24-well culture plate at a density of 5×10^4 cells/cm^2 (Corning, NY, NY, USA). The bEnd3 cells were seeded on the luminal side of the collagen-coated polyester membrane of the inserts (0.4 μm mean pore size) at a density of 4×10^4 cells/cm^2 (Millipore). The seeded cells were allowed to grow at 37°C in a 5% CO$_2$/95% air atmosphere until they reached 80%–90% confluence. Then, the inserts were placed in the wells of 24-well culture plates containing astrocytes to co-cultured together for 24 h, and then prepared for oxygen and glucose deprivation/reperfusion (OGD/R) experiments.

2.16 | Oxygen and glucose deprivation/reoxygenation

Oxygen and glucose deprivation/reoxygenation (OGD/R) treatment was performed as previously described (Peng et al., 2020; Wang et al., 2020). Astrocytes were rinsed twice with PBS and incubated in glucose-free DMEM (Invitrogen) in a hypoxia incubator (Thermo Fisher Scientific, Waltham, MA, USA). The incubator was flushed with gas (1% O$_2$, 5% CO$_2$, balanced with N$_2$). The plates were then transferred to the hypoxia incubator and left in OGD conditions (1% O$_2$,

5% CO_2, balanced with N_2) for a further 4 h. After OGD, the serum-free and glucose-free medium was replaced with glucose-containing DF12. Then, the OGD cells were returned to normal conditions (95% air and 5% CO_2) for 20 h of reperfusion.

2.17 | Drug treatment

Adult mice received a single intravenous injection (i.v.) injection of 50 mg/kg LM11A-31 dihydrochloride (CAS: 1243259-19-9; MedChem Express, New Jersey, USA) immediately after the reperfusion of the MCAO operation (Elshaer et al., 2019; Knowles et al., 2013; Simmons et al., 2016). The LM11A-31 ((2S,3S)-2-Amino-3-methyl-N-[2-(4-morpholinyl)ethyl] pentanamide dihydrochloride) was obtained from MedChem Express (New Jersey, USA) at >98.0% purity, and the structure was confirmed by liquid chromatography/mass spectroscopy (LC–MS/MS) analysis. The LM11A-31 was diluted in saline. Control mice received a single i.v. injection of saline under the same conditions.

In vitro, LM11A-31 was dissolved in PBS to a concentration of 10 mM (10,000× stock solution) and diluted in DF12 medium to a final concentration of 1 μM before use. The γ-secretase inhibitor (Compound E), NF-κB p65 inhibitor (JSH-23), and HIF-1α inhibitor (PX-478) (209986-17-4, 749,886-87-1, and 685,898-44-6, respectively, MedChem Express) were separately dissolved in dimethyl sulfoxide and diluted in DF12 medium to a final concentration of 1 μM (Le Moan et al., 2011; Schachtrup et al., 2015), 10 μM (Shin et al., 2014), and 20 μM (Fernandez Esmerats et al., 2019) respectively. The inhibitors were separately added to astrocytes 10 min before OGD and reoxygenation treatment. The control group received the same volume of solvent with the same administrative methods, at the same time of drug administration.

2.18 | In vitro BBB permeability assay

Permeability of the in vitro BBB model was measured as previously described (Kuo et al., 2019; P. Wang et al., 2021). In brief, after OGD/R treatment, 750 μl DF12 medium was added to each lower chamber and 150 ml DF12 medium containing 1 mg/ml fluorescein isothiocyanate-dextran (FITC-dextran 70 kDa; Invitrogen) was added to each insert (luminal chamber). After incubation for 2 h at 37°C in 5% CO_2/95% air, the insert was removed. Aliquots of 200 μl conditioned medium (CM) from the abluminal chamber were collected and the fluorescence intensity at 520 nm was measured using a microplate reader (Bio-Rad, Hercules, CA, USA).

2.19 | Cultures of bEnd.3 cells with different types of astrocyte conditioned medium

After culturing under normal culture conditions to 80%–90% confluence, bEnd.3 cells were cultured with different types of astrocyte-conditioned medium (ACM) during OGD and reoxygenation processes (Shan et al., 2019). The grouping of the bEnd.3 cells treated with ACM was based on astrocyte treatment and included normal O_2 group, the OGD/R blank group, the OGD/R + LM11A-31 group, the OGD/R + Compound E group, the OGD/R + JSH-23 group, and the OGD/R + PX-478 group.

2.20 | Measurement of cell viability

The cell viability was evaluated by using the CCK-8 assay kit (Dojindo, Kumamoto, Japan) following the manufacturer's instructions (Peng et al., 2020). 10 μl CCK-8 assay Kit was added into 100 μl cell culture medium in the 96-well plates and cultured at 37°C for up to 4 h. The fluorescence intensity was measured using a microplate reader (Bio-Rad, Hercules, CA, USA) at an absorbance of 450 nm.
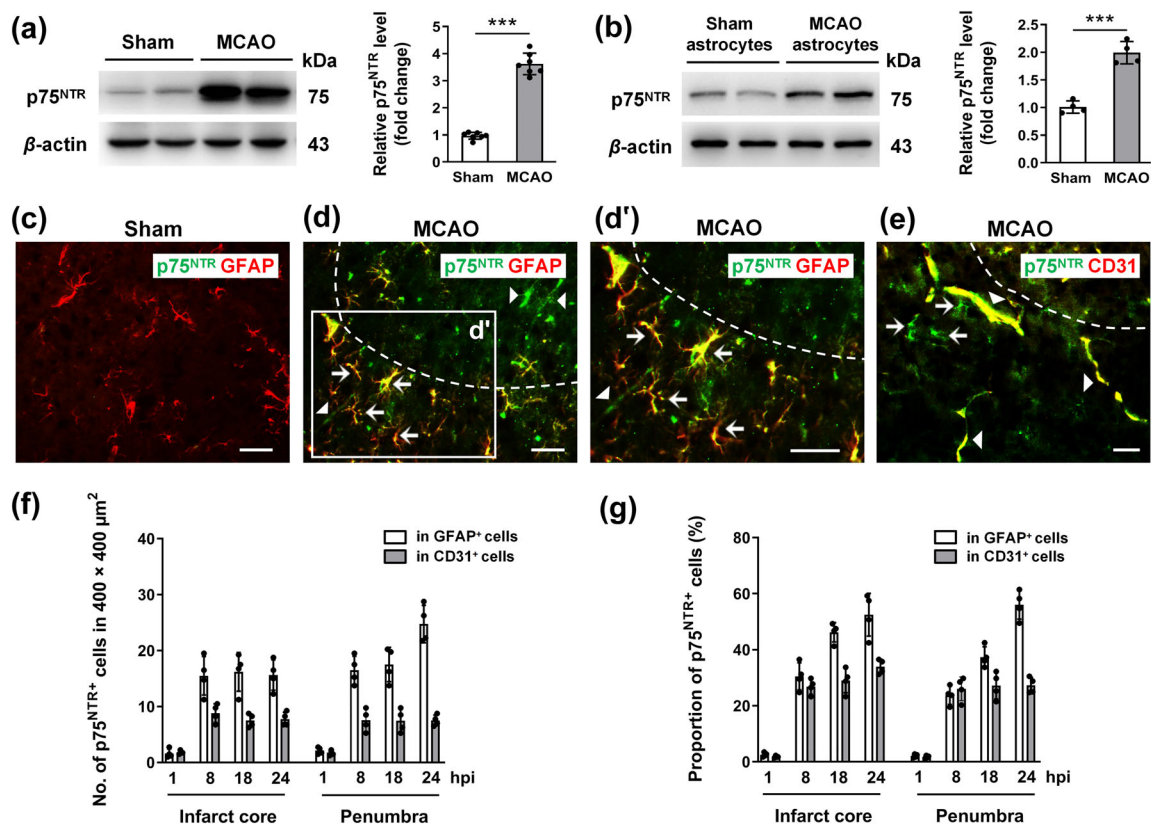
2.21 | Statistical analysis

GraphPad Prism software, version 6.0 (USA) was used for statistical analysis, and the results were presented as a mean ± SD. Individual comparisons were assessed using an unpaired Student's t-test, and multiple comparisons were performed using one-way analysis of variance with Tukey's post hoc tests. All tests were considered statistically significant at $p < .05$. $^*p < .05$; $^{**}p < .01$; $^{***}p < .001$.

3 | RESULTS

3.1 | p75[NTR] deficiency ameliorates stroke-induced brain tissue damage and BBB breakdown

To investigate the role of p75[NTR] on BBB permeability in ischemic stroke, firstly we evaluated p75[NTR] expression in the ipsilateral cortices after inducing stroke in the mice using a transient MCAO model (Zhang, Tang, et al., 2020) (Figure 2a, Figure S1). In line with previous reports (Irmady et al., 2014), the Western blot results showed that p75[NTR] expression was indeed increased in the ipsilateral cortices at 24 h after stroke (vs. the sham group, $^{***}p < .001$) (Figure 2a). To verify the involvement of p75[NTR] on BBB disruption, we induced MCAO in p75[NTR+/−] mice and their WT littermates (Figure 1a, Figure S4a). At 24 h after ischemia reperfusion, smaller infarct volumes was observed in p75[NTR+/−] mice compared to the WT (WT: 40.15 ± 10.44%; p75[NTR+/−]: 21.48 ± 4.47%) (Figure 1b,c). In addition, both the brain edema volumes (WT: 7.96 ± 3.65%; p75[NTR+/−]: 3.98 ± 2.31%) (Figure 1d) and EB dye extravasation (WT: 10.16 ± 2.72 μg/g; p75[NTR+/−]: 4.25 ± 1.53 μg/g) (Figure 1e,f) were reduced in p75[NTR] knockdown mice, suggesting p75[NTR] is involved in the BBB disruption after ischemic stroke. We further assessed the expression of TJ proteins in the infarct cores and penumbra of p75[NTR+/−] and WT mice by

immunostaining of CD31 and ZO-1/occludin (OCLN) (Figure 1g,h,j). The MFI of ZO-1 and OCLN in the infarct cores (relative MFI of ZO-1: WT, 0.27 ± 0.037; p75$^{NTR+/-}$, 0.41 ± 0.046; *p < .05; OCLN: WT, 0.26 ± 0.058; p75$^{NTR+/-}$, 0.43 ± 0.042; *p < .05) as well as in the penumbra was increased in p75$^{NTR+/-}$ mice after MCAO (Figure 1h–k) (ZO-1: WT, 0.45 ± 0.043; p75$^{NTR+/-}$, 0.58 ± 0.061; *p < .05; OCLN: WT, 0.42 ± 0.052; p75$^{NTR+/-}$, 0.55 ± 0.049; *p < .05), indicating a better preserved TJ protein expression in the mutant mice. Taken together, these results suggested that provoked p75^{NTR} expression after ischemic stroke contributed to the brain pathology including cerebrovascular impairment, while genetic knockdown of p75^{NTR} ameliorated the BBB function after cerebral ischemia.

3.2 | The p75^{NTR} expression is upregulated in astrocytes and endothelial cells after ischemic brain injury

To identify the cellular source of p75^{NTR}, we performed immunostaining in the ipsilateral brain combining p75^{NTR} and cell specific markers (Cheng et al., 2018; Saadipour et al., 2018). To determine the dynamic changes of p75^{NTR} expression after MCAO, we performed IHC to brain slices acquired at 1, 8, 18, and 24 h post injury (hpi). In line with previous studies (Andsberg et al., 2001; Angelo et al., 2009; Park et al., 2000), we observed the p75^{NTR} expression in the ischemic area particularly in neurons already at 1 hpi (Figure S2b). From as early as at least 8 hpi, we also found a number of p75^{NTR+} cells bearing

FIGURE 1 The p75^{NTR} deficiency ameliorates stroke-induced brain tissue injury, brain edema, and blood–brain barrier breakdown. (a) Western blot analysis and quantification of p75^{NTR} in the cerebral cortices of WT and p75$^{NTR+/-}$ mice at 24 hr after MCAO operation. $N = 4$ for both groups. (b) Representative images of TTC staining in WT and p75$^{NTR+/-}$ mice. Each group, $N = 6$. (c) Quantitative analysis of infarct volume (as a percentage of the ipsilateral hemisphere) in WT and p75$^{NTR+/-}$ mice. $N = 6$. (d) Quantitative analysis of relative edema volumes by measuring ischemic hemispheric enlargements in WT and p75$^{NTR+/-}$ mice. $N = 6$. (e, f) representative brain slices showed Evans blue (EB) extravasation (blue dye leakage) (top) and quantitative analysis of EB content in ischemic hemispheres (bottom) in WT and p75$^{NTR+/-}$ mice. $N = 7$. (g) the schematic diagram of the area chosen to be analyzed in the immunofluorescent staining experiment. (h–k) Immunofluorescence co-staining of ZO-1 (green) and CD31 (red) (h, i) and immunofluorescence co-staining of occludin (OCLN) (green) and CD31 (red) (j, k) in infarct cores and penumbra in the ischemic cortices of WT and p75$^{NTR+/-}$ mice. Scale bars = 50 μm. Relative mean fluorescence intensity (MFI) of ZO-1 / MFI of CD31 in CD31$^+$ cells and relative MFI of OCLN/CD31 in CD31$^+$ cells were shown on the right side. Total around 120 CD31$^+$ cells per mice were counted. $N = 3$. Data are expressed as the mean ± SD. *p < .05; **p < .01; ***p < .001; *ns*, not significant. MCAO, middle cerebral artery occlusion; MFI, mean fluorescence intensity; OCLN, occludin; ZO-1, zonula occludens-1

FIGURE 2 The expression of p75^{NTR} in the cerebral cortices after ischemic brain injury. (a) Western blot analysis and quantification of p75^{NTR} in the cerebral cortices of wild-type mice 24 hr after sham or middle cerebral artery occlusion (MCAO) operation. $N = 7$. (b) Western blot analysis and quantification of p75^{NTR} expression in MACS-sorted astrocytes obtained from the ischemic cortices of the wild-type sham and MCAO mice. $N = 4$. (c, d) representative immunofluorescent co-staining of p75^{NTR} (green) and GFAP (red) in the cortices of the sham and MCAO mice. (d') large magnification image of the section marked in the white rectangle. The separation of the infarct cores and penumbra was marked by the dash lines, top: Infarct cores, bottom: Penumbra. Arrows: p75^{NTR+} cells showed astrocyte-like morphology. Arrow heads: p75^{NTR+} cells showed blood vessel-like morphology. Scale bars = 50 μm. (e) Immunofluorescent co-staining of p75^{NTR} (green) and CD31 (red) in the cortices of stroke mice. The separation of the infarct cores and penumbra was marked by the dash lines, top: Infarct cores, bottom: Penumbra. Arrows: p75^{NTR+} cells showed astrocyte-like morphology. Arrow heads: p75^{NTR+} cells showed blood vessel-like morphology. Scale bar = 100 μm. (f) Number of p75^{NTR+} GFAP$^+$ or p75^{NTR+} CD31$^+$ cell in 400 × 400 μm^2. Total around 600 cells per mice were counted. $N = 4$. (g) Proportion of p75^{NTR+} GFAP$^+$ or p75^{NTR+} CD31$^+$ double positive cells in GFAP$^+$ or CD31$^+$ single positive cell. $N = 4$. Data are expressed as the mean ± SD. $*p < .05$; $**p < .01$; $***p < .001$. [Correction added on January 28, 2022, after first online publication: Figure 2 has been updated with revised version]

astrocyte-like or vascular morphology both in the infarct cores and penumbra, but not in the uninjured area or in the brains of sham mice (Figure 2c–e, Figure S2a,c,d). Double immunostaining of p75^{NTR} and GFAP (astrocyte marker)/CD31 (endothelial cell marker) confirmed that indeed a subset of astrocytes and endothelial cells upregulated the expression of p75^{NTR} in the ischemic area (Figure S2c,d). Further quantification demonstrated that although the density of p75^{NTR+}GFAP$^+$ astrocytes (cell number in 400 × 400 μm^2) did not change in the ischemic core but slightly increased from ~16.5 (8 hpi) to ~25 (24 hpi) in the penumbra, the proportion of GFAP$^+$ astrocytes expressing p75^{NTR} increased gradually from 8 to 24 hpi both in the ischemic core and penumbra (from ~30% to ~52% and from ~24% to ~56%, respectively) (Figure 2f,g). However, both the density and the proportion of CD31$^+$ endothelial cells expressing p75^{NTR} maintained at the same level over time (about 30% and 27% in the infarct core and penumbra,

respectively) (Figure 2f,g). In addition, p75^{NTR} immunoblot signals were increased in the MAC-sorted cortical astrocytes of stroke mice ($***p < .001$) at 24 hpi (Figure 2b, Figure S4b), further confirming the upregulation of p75^{NTR} in astrocytes triggered by cerebral ischemia. Taken together, our results suggested that in addition to neurons, a significant number of astrocytes and endothelial cells expressed p75^{NTR} already at early stage after ischemic injury.

3.3 | Astrocyte-specific knockdown of p75^{NTR} mitigates ischemia-induced brain tissue injury and improves neurological functions after stroke

To investigate the role of astrocytic p75^{NTR} on ischemic brain injury, an AAV containing pAKD-CMV-bGlobin-FLEX-miR30-sh-p75^{NTR}
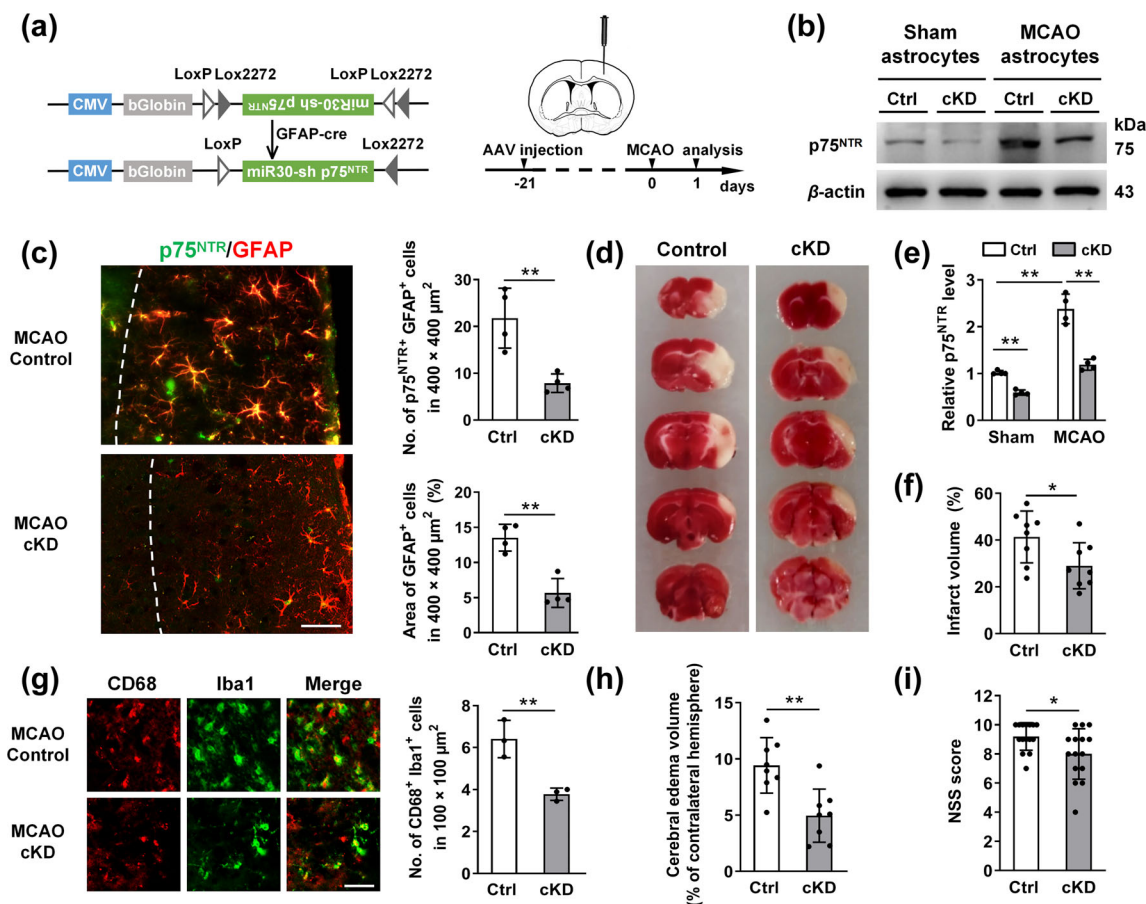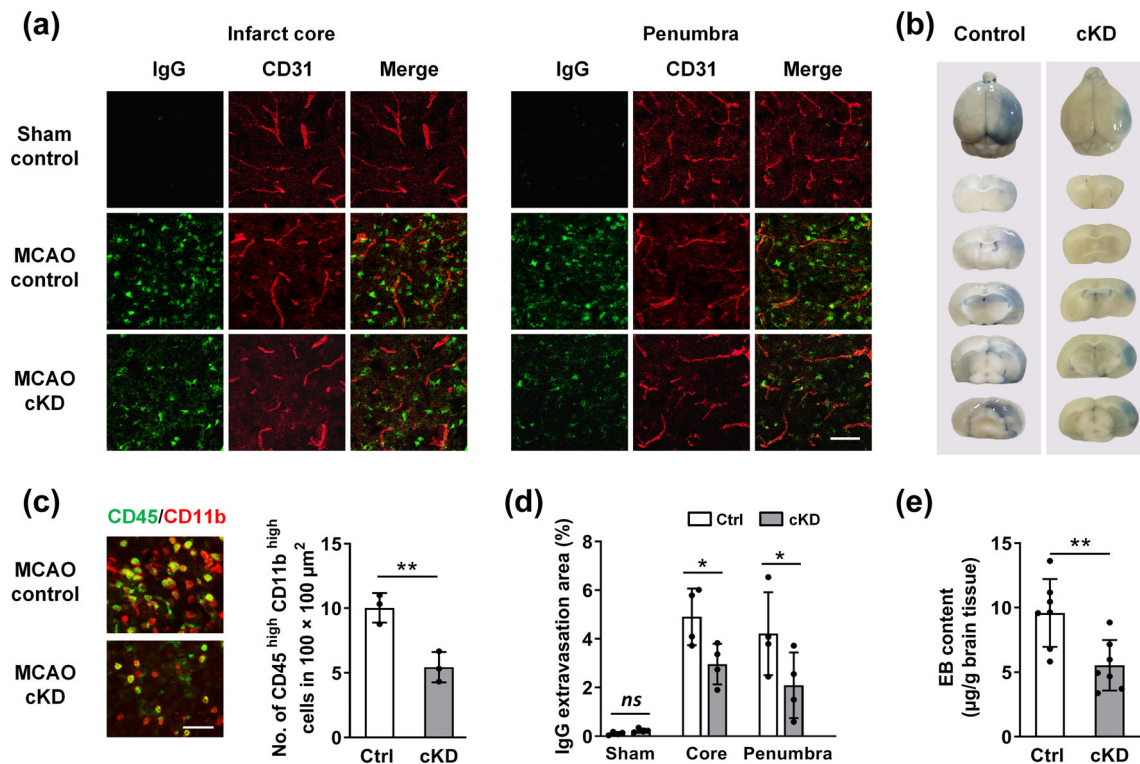
FIGURE 3 Astrocyte-conditional knockdown of p75^NTR mitigates ischemia-induced glia activation, brain tissue injury and improves neurological functions after stroke. (a) The schematic diagram showing how the p75^NTR knockdown adeno-associated virus (AAV) targeting astrocytes to achieve astrocyte-conditional knockdown of p75^NTR. 21 days before MCAO operation, the AAV (pAKD-CMV-bGlobin-Flex-p75^NTR-miR30-shRNA) was injected into the GFAP-cre mice. The reversed sequence of miR30-shRNA of p75^NTR was inserted between 2–LoxP-Lox2272–sequence and would flanked to express the shRNAs of p75^NTR when meet the cre enzymes. (b) Western blot analysis and (e) quantification of p75^NTR expression in MACS-sorted astrocytes obtained from the ischemic cortices of the mice injected with control AAV or astrocyte p75^NTR conditional knockdown (p75^NTR cKD, cKD) AAV. $N = 4$. (c) Immunofluorescent staining of p75^NTR (green) and GFAP (red) and quantification of p75^NTR+ GFAP+ astrocytes and the area percentage of GFAP+ activated astrocytes in the infarct cores of the mice cortices in control and p75^NTR cKD mice. The infarct cores were marked by the dash lines, left: Uninjured area, right: Infarct cores. Scale bar = 50 μm. $N = 4$. (d) Representative TTC staining of mice brains in control mice and p75^NTR cKD mice. (f) Quantitative analysis of infarct volumes. $N = 8$. (g) Immunofluorescent staining and quantitative analysis of CD68 (red) and Iba1 (green) double positive cells in the infarct-affected area in cortices. Scale bars = 50 μm. $N = 3$. (h) Quantitative analysis of relative edema volumes by measuring ischemic hemispheric enlargements. $N = 8$. (i) Neurological severity scores indicating neurological functions. $N = 15$. Data are expressed as the mean ± SD. *$p < .05$; **$p < .01$; ***$p < .001$. Ctrl, control; cKD, p75^NTR cKD, astrocyte-specific p75^NTR conditional knockdown

vector was injected into the deep dorsal cortex of GFAP-cre mice to achieve specific silencing of p75^NTR in astrocytes (astrocyte-specific p75^NTR conditional knockdown, p75^NTR cKD) (Figure 3a). Western blot results indicated this AAV-mediated p75^NTR cKD approach caused a ~40% reduction of p75^NTR expression in MAC-sorted astrocytes under the basal conditions (Figure 3b,e). After MCAO insult, the increase of p75^NTR expression in cortical astrocytes was also significantly attenuated by ~55% in p75^NTR cKD mice, compared with those treated with the control AAV (Figure 3b,e). In line with the Western blot results, IHC experiments revealed that the number of p75^NTR+ GFAP+ double positive astrocytes in the infarct-affected area of p75^NTR cKD mice decreased significantly (Figure 3c) (cell number in

400×400 μm², Ctrl: 21.78 ± 6.39; p75^NTR cKD: 7.88 ± 1.97), indicating a successful knockdown of p75^NTR in astrocytes.

Then, we assessed the activation of astrocytes by measuring the area occupied by GFAP+ astrocytes in the infarct-affected cortices and found that p75^NTR cKD reduced astrocyte activation (Ctrl: 13.53 ± 1.90%; p75^NTR cKD: 5.66 ± 2.06%) (Figure 3c). Astrocytic p75^NTR knockdown also decreased the number of activated microglia (CD68+ Iba1+) in the infarct-affected cortices (Figure 3g) (Ctrl: 6.41 ± 0.89; p75^NTR cKD: 3.78 ± 0.29). Subsequently, we further determined post-stroke outcomes in p75^NTR cKD mice. The results showed that the infarct volumes (Ctrl: 41.34 ± 11.08%; p75^NTR cKD: 29.01 ± 9.84%, *$p < .05$) (Figure 3d,f) and cerebral edema volumes (Ctrl: 9.42

FIGURE 4 Astrocyte-conditional knockdown of p75^{NTR} ameliorats BBB disruption after stroke. (a, d) immunofluorescence staining and quantitative analysis of IgG extravasation into the parenchyma in the infarct cores and penumbra of control and p75^{NTR} cKD mice. Scale bar = 50 μm. $N = 4$. (b, e) representative EB staining images and quantitative analysis of EB content in ischemic hemispheres in control mice and p75^{NTR} cKD mice. $N = 7$. (c) Immunofluorescent staining and quantification of CD45 (green) high expressing and CD11b (red) high expressing cells in the infarct area of ischemic cortices. Scale bars = 50 μm. $N = 3$. Data are expressed as the mean ± SD. *$p < .05$; **$p < .01$; ***$p < .001$; ns, not significant. Ctrl, control; cKD, p75^{NTR} cKD, astrocyte-specific p75^{NTR} conditional knockdown

± 2.47%; p75^{NTR} cKD: 4.96 ± 2.36%, **$p < .01$) (Figure 3h) were significantly smaller in p75^{NTR} cKD mice (vs. the control mice). Furthermore, the p75^{NTR} cKD mice had lower NSS (Ctrl: 9.20 ± 0.94; p75^{NTR} cKD: 8.00 ± 1.73, *$p < .05$), indicating improved neurological functions after stroke (Figure 3i). These results revealed that astrocyte p75^{NTR} contributed to the ischemia-induced brain tissue injury after stroke.

3.4 | Knockdown of astrocytic p75^{NTR} ameliorates BBB disruption after ischemic stroke

Since astrocytes regulate BBB integrity and p75^{NTR} increases vascular permeability of the blood-retinal barrier in hypoxia conditions (Barcelona et al., 2016; Le Moan et al., 2011), we asked whether astrocytic p75^{NTR} affected BBB integrity after ischemic stroke. We assessed BBB permeability by measuring the amounts of EB dye and autogenous IgG leakage in the brain parenchyma. Acute cerebral ischemia-induced robust BBB leakage of EB dye in the infarct area of control mice, whereas astrocytic p75^{NTR} knockdown reduced EB extravasation (Ctrl: 9.59 ± 2.62 μg/g; p75^{NTR} cKD: 5.53 ± 1.95 μg/g, **$p < .01$) (Figure 4a,d). In parallel, the extravasation of autogenous IgG in the infarct cores (Ctrl: 4.91 ± 1.17%;

p75^{NTR} cKD: 2.96 ± 0.83%) and penumbra (Ctrl: 4.22 ± 1.70%; p75^{NTR} cKD: 2.09 ± 1.35%) was also reduced in p75^{NTR} cKD mice (Figure 4b,e). Given that tight junction proteins between endothelial cells are vital for the maintenance of the BBB integrity (Jiao et al., 2011; Sandoval & Witt, 2008), the effect of astrocytic p75^{NTR} on the loss of tight junctions following cerebral ischemia was evaluated. Western blot results showed a protection of tight junction proteins ZO-1 (*$p < .05$) and OCLN (*$p < .05$) in the ischemic cortices of p75^{NTR} cKD mice (Figure 5a,b). IHC results revealed that relative MFIs of ZO-1 and OCLN were significantly higher in the infarct cores (ZO-1: 0.28 ± 0.046 in contol group, 0.40 ± 0.035 in p75^{NTR} cKD group; OCLN: 0.27 ± 0.036 in contol group, 0.43 ± 0.049 in p75^{NTR} cKD group) and in the penumbra (ZO-1: Ctrl, 0.47 ± 0.048; p75^{NTR} cKD, 0.58 ± 0.054; OCLN: Ctrl, 0.41 ± 0.046; p75^{NTR} cKD, 0.59 ± 0.064) in p75^{NTR} cKD mice (Figure 5c–f), suggesting that knockdown of astrocytic p75^{NTR} preserved tight junctions after brain ischemic injury. In addition, by analyzing the leukocyte infiltration caused by BBB disruption (Li et al., 2018; Sifat et al., 2017), we observed that astrocytic p75^{NTR} knockdown significantly reduced the infiltration of leukocytes (CD45 high expressing and CD11b high expressing, CD45^{high} CD11b^{high} cells) around the infarct cores (Figure 4c) (cell number in 100 × 100 μm^2, Ctrl: 10.04
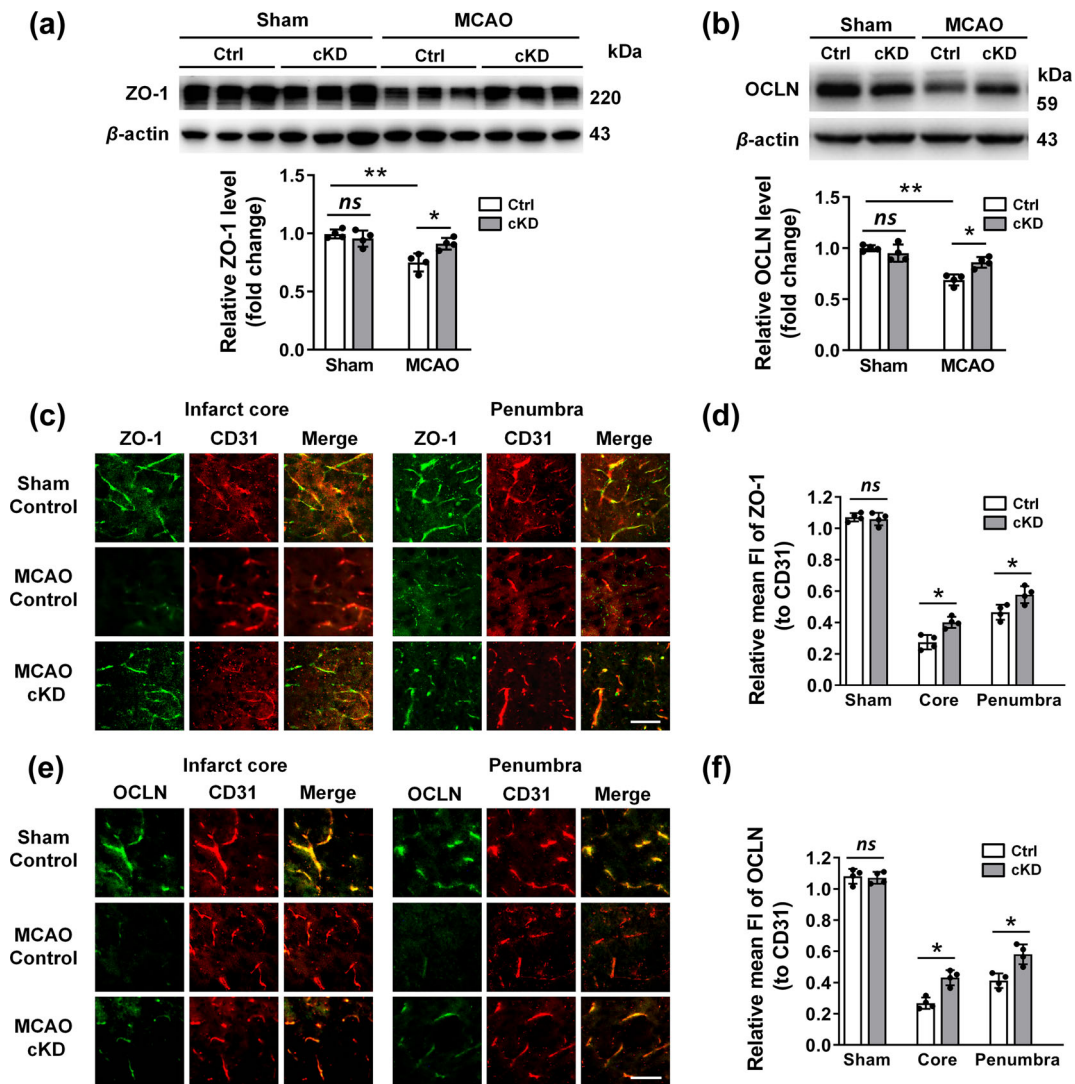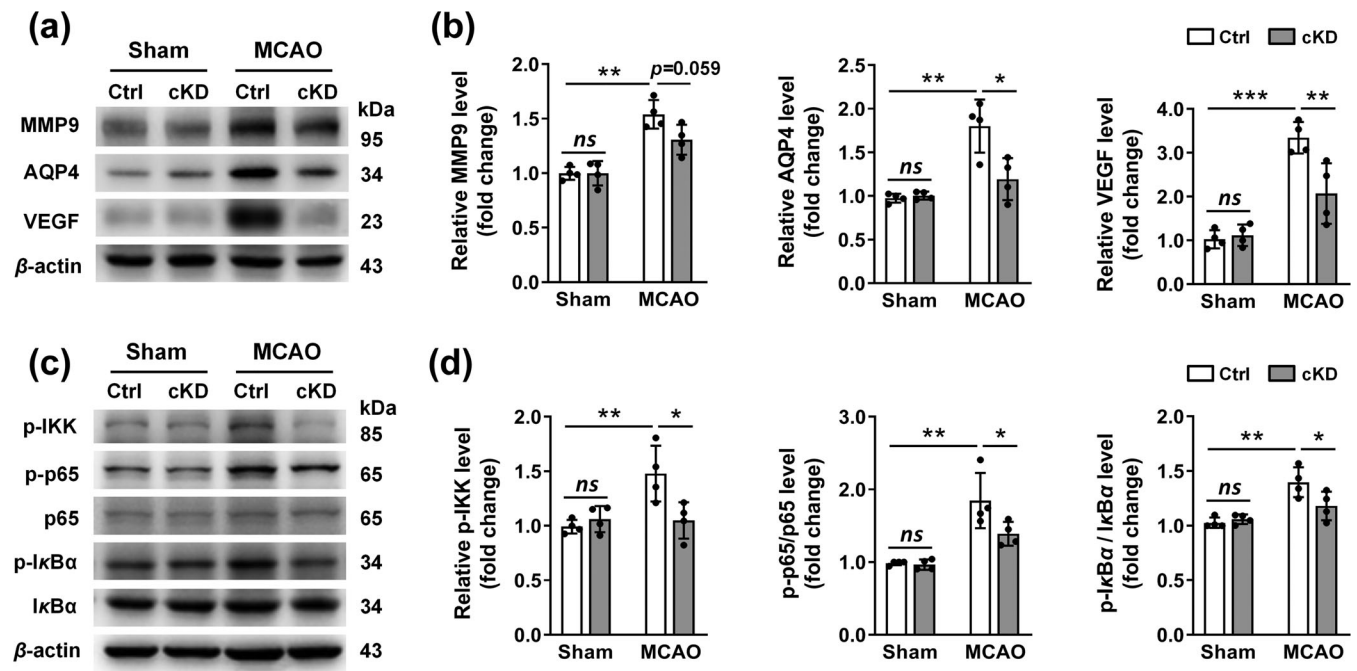
FIGURE 5 Knockdown of astrocytic p75^{NTR} inhibits tight junction disruption after stroke. (a, b) Western blot analysis and quantification of (a) ZO-1 and (b) occludin expression in the cortices of mice injected with control AAV and p75KD AAV. $N = 4$. (c, d) Immunofluorescent co-staining and quantitative analysis of ZO-1 (green) and CD31 (red) in the infarct cores and penumbra of mice injected with control AAV and p75^{NTR} cKD AAV. Scale bars = 50 μm. $N = 4$. (e, f) immunofluorescence co-staining and quantitative analysis of occludin (green) and CD31 (red) in the infarct cores and penumbra of control and p75^{NTR} cKD mice. Scale bars = 50 μm. $N = 4$. Data are expressed as the mean ± SD. *$p < .05$; **$p < .01$; ***$p < .001$. *ns*, not significant. Ctrl, control; OCLN, occludin; ZO-1, zonula occludens-1; cKD, p75^{NTR} cKD, astrocyte-specific p75^{NTR} conditional knockdown

± 1.14; p75^{NTR} cKD: 5.44 ± 1.17). Taken together, these results suggested that activation of astrocytic p75^{NTR} deteriorated BBB leakage after ischemic stroke.

3.5 | Astrocytic p75^{NTR} impairs tight junctions of BBB after ischemic injury via NF-κB signaling

Previous studies demonstrated that astrocyte-derived MMP9 and VEGF contribute to the degradation of tight junctions, thereby directly causing BBB breakdown (Argaw et al., 2012; Zhang et al., 2018). As well, the water channel protein AQP4 facilitates brain edema after stroke

(Filchenko et al., 2020). Therefore, we assessed the influence of p75^{NTR} on expression of MMP9, VEGF, and AQP4 in MAC-sorted astrocytes from p75^{NTR} cKD mice by Western blot analysis. Ischemic injury significantly elevated astrocytic MMP9 (**$p < .01$), VEGF (***$p < .001$), and AQP4 (**$p < .01$) protein expression which was attenuated by p75^{NTR} cKD (**$p < .01$, *$p < .05$ for VEGF, AQP4, respectively; and a strong tendency to inhibit MMP9, $p = .0586$) (Figure 6a,b). In addition, a gelatin zymography assay (a well-established assay for MMP activity, especially MMP9) showed a decreased MMP9 activity (*$p < .05$) in brain homogenates of p75^{NTR} cKD mice than the control mice after MCAO, indicating astrocyte p75^{NTR} knockdown reduced the expression of MMP9 (Figure S3).

FIGURE 6 Knockdown of astrocytic p75^{NTR} downregulats MMP-9, AQP4, VEGF, and NF-κB signals after stroke. (a, b) Western blot analysis and quantification of astrocytic MMP9, AQP4 and VEGF expression in astrocytes MAC-sorted from the ischemic cortices of control and p75^{NTR} cKD mice. $N = 4$. (c, d) Western blot analysis and quantification of astrocytic p-IKK expression and phosphorylation of NF-κB p-65 and phosphorylation of IκBa in astrocytes MAC-sorted from control and p75^{NTR} cKD mice. $N = 4$. Data are expressed as the mean ± SD. $*p < .05$; $**p < .01$; $***p < .001$.; ns, not significant. Ctrl, control; cKD, p75^{NTR} cKD, astrocyte-specific p75^{NTR} conditional knockdown. [Correction added on January 28, 2022, after first online publication: Knockdown of astrocytic p75NTR downregulats MMP-9, AQP4, VEGF, and NF-κB signals stroke. this has been updated]

The intracellular domain (ICD) of p75^{NTR} activates NF-κB signaling (Caporali et al., 2015; Yuan et al., 2019), which is involved in many inflammation related biopathological processes, including ischemic stroke (Fann et al., 2018; Sivandzade et al., 2019). Furthermore, MMP9 and VEGF has been shown to be upregulated in inflammatory status via activation of NF-κB signaling pathway (Pan et al., 2020; Qin et al., 2019; Wu et al., 2020). The p65 is a member of the NF-κB protein family, which is usually binded and inhibited by IκB protein in health (Harari & Liao, 2010). However, after ischemic stroke, proinflammatory cytokines and other endogenous danger signals activate the IκB kinase (IKK) complex, which phosphorylates IκBα and leads to ubiquitination and proteasomal degradation of IκBα to release p65 (Howell & Bidwell, 2020; Zhan et al., 2016). Hence, we examined the phosphorylation level of p65 and IκBα in astrocytes from control and cKD animals. We found that ischemic stroke promoted phosphorylation of p65 ($**p < .01$) and IκBα ($**p < .01$) in the MAC-sorted astrocytes from ipsilateral cortices of control animals, whereas the increase in the p75^{NTR} cKD astrocytes were mitigated ($*p < .05$, $*p < .05$, respectively) (Figure 6c,d). Since IκBα is degraded by p-IKK, we also tested the level of p-IKK. The p-IKK was upregulated in the control astrocytes ($**p < .01$), while cKD of p75^{NTR} retarded the upregulation ($*p < .05$) (Figure 6c,d). These results suggested that astrocytic p75^{NTR} increased the expression and phosphorylation of IKK, degraded IκBα and subsequently augmenting phosphorylation and activation of NF-κB signaling pathway. Altogether, current results strongly suggest that astrocytic p75^{NTR} impaired BBB integrity by upregulating MMP9 and VEGF expression via the NF-κB signaling pathway.

3.6 | Astrocytic p75^{NTR} leads to OGD-induced BBB disruption in vitro

To further investigate the mechanisms of astroglial p75^{NTR} regulating BBB integrity, in vitro OGD and reoxygenation (OGD/R) model was used to mimic the stroke situations (Peng et al., 2020). Similar to stroke insult, OGD/R exposure significantly upregulated p75^{NTR} expression ($***p < .001$) in astrocytes (Figure 7a). For the study of in vitro BBB integrity, a model consisting of bEend.3 endothelial cells and astrocytes (Figure 7c) was used. Astrocytes were cultured in the 24-well plates and bEend.3 cells were cultured on the luminal side of transwell inserts to generate a co-culture system. The p75^{NTR} expression in astrocytes was silenced by siRNA before co-culturing with bEend.3 endothelial cells, which led to about 70% of depletion efficiency (vs. the scrambled siRNA, si Ctrl) (Figure 7b). Meanwhile, p75^{NTR} siRNA and p75^{NTR} overexpression (p75 OE) did not affect cell viability of astrocytes after OGD/R (si Ctrl: 55.90 ± 6.33%; si p75: 57.51 ± 11.12%; Ctrl: 53.55 ± 4.30%; p75 OE: 49.45 ± 11.97%) (Figure S4c,d). First, we analyzed the BBB permeability by measuring FITC-dextran leakage to the lower chamber after OGD/R ($***p < .001$). The fluorescence intensity of FITC-dextran
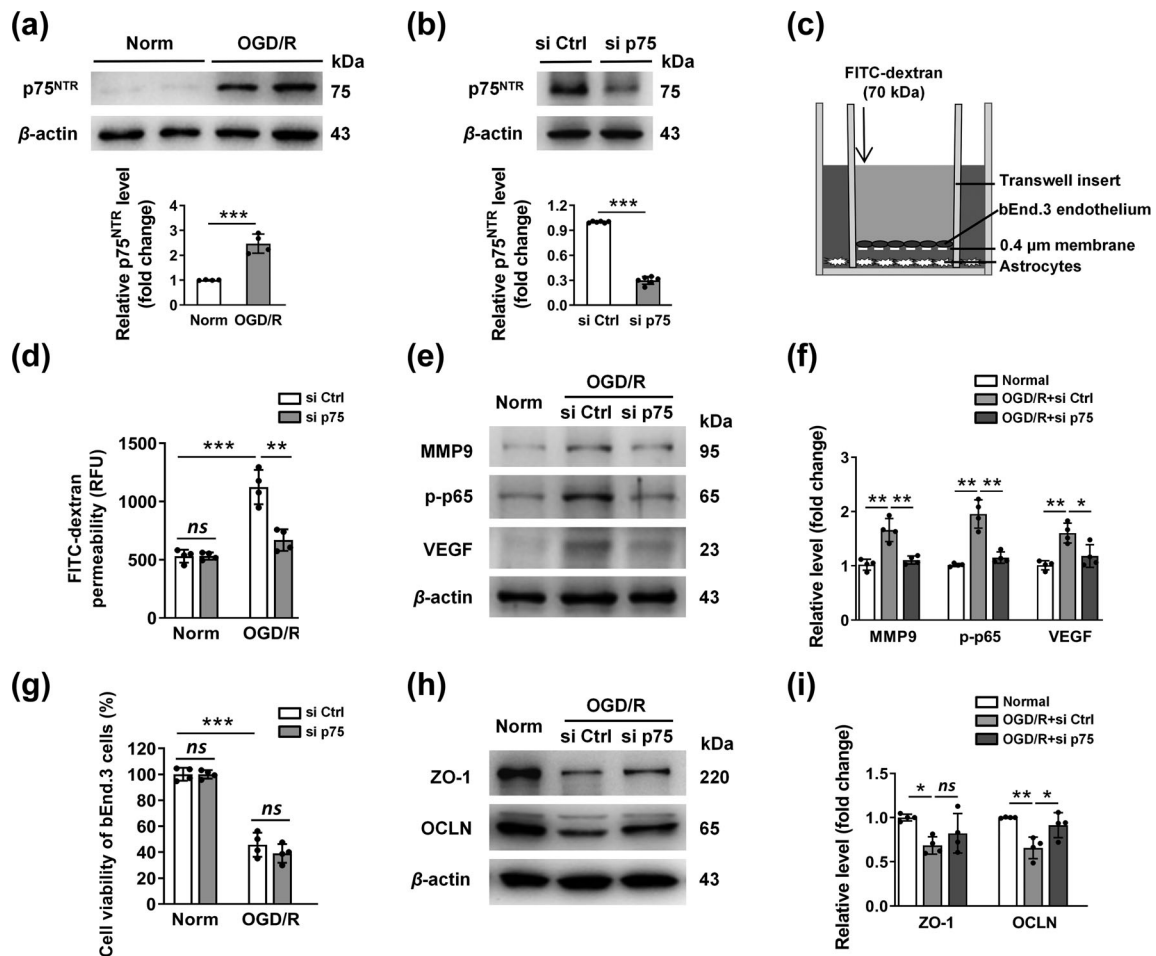
FIGURE 7 siRNA of p75^NTR preservs tight junction protein expression and thus protects the in vitro blood–brain barrier (BBB) integrity after OGD reoxygenation. (a, b) Western blot analysis and quantification of p75^NTR expression in normal conditions or after OGD and reoxygenation (OGD/R). The p75^NTR expression was increased after OGD/R and OGD-induced p75^NTR expression was inhibited by siRNA of p75^NTR (si p75) versus the scrambled control siRNA (si ctrl). N = 4. (c) The schematic diagram of the in vitro BBB model. (d) In vitro BBB permeability to FITC-dextran (70 kDa) when using astrocytes transfected with si ctrl or si p75. N = 4. (e, f) Western blot analysis and quantification of MMP-9, VEGF, and p–p65 expression in astrocytes from the in vitro BBB, which were transfected with si ctrl or si p75. N = 4. (g) Cell viability of bEnd.3 endothelial cells co-cultured with conditioned medium from astrocytes transfected with si ctrl or si p75 in normal conditions or exposed to OGD/R. N = 4. (h, i) Western blot analysis and quantification of ZO-1 and occludin expression in bEnd.3 endothelial cells after OGD/R when added conditioned medium from astrocytes during the OGD/R processes. Data are expressed as the means ± SD. *$p < .05$; **$p < .01$; ***$p < .001$; ns, not significant.Norm, normal O_2 conditions; OGD/R, oxygen and glucose deprivation/reoxygenation; si ctrl, scramble siRNA; si p75, siRNA of p75^NTR; OCLN, occludin; ZO-1, zonula occludens-1

increased in the control system (co-cultured with control astrocyte), while that in the knockdown condition (co-cultured with p75^NTR knockdown astrocytes) was significantly attenuated (si Ctrl: 1124.72 ± 147.71; si p75: 668.85 ± 92.79, **$p < .01$) (Figure 7d). In addition, the p75^NTR silencing significantly attenuated the upregulation of p-p65, MMP9 and VEGF (**$p < .01$, **$p < .01$, *$p < .05$, respectively) in astrocytes in the in vitro BBB model following OGD/R (Figure 7e,f).

Then we evaluated the impact of astroglial p75^NTR on the endothelial cells analyzing the tight junction proteins of the bEend.3 cells after adding the CM (conditioned medium) of astrocytes (transfected with the scrambled siRNA or the p75^NTR siRNA) during the OGD/R

processes. When exposed to OGD/R, the cell viability of bEend.3 endothelial cells was not affected by the astroglial CM (transfected with the scrambled siRNA 39.06 ± 7.25% or p75^NTR siRNA 45.76 ± 9.31%) (Figure 7g), suggesting astrocytic p75^NTR do not affect apoptosis of endothelial cells in hypoxia condition. However, the CM of KD astrocytes preserved OCLN expression in bEend.3 cells compared with control CM (vs. the scrambled siRNA, *$p < .05$) (Figure 7h,i). In addition, a slight increase of ZO-1 protein expression ($p = .3032$) was observed in the p75^NTR siRNA group (Figure 7h,i), no significance though. Thus, our results suggested that astrocytic p75^NTR facilitated MMP9 and VEGF expression, contributing to the tight junction impairment and subsequent BBB disruption.
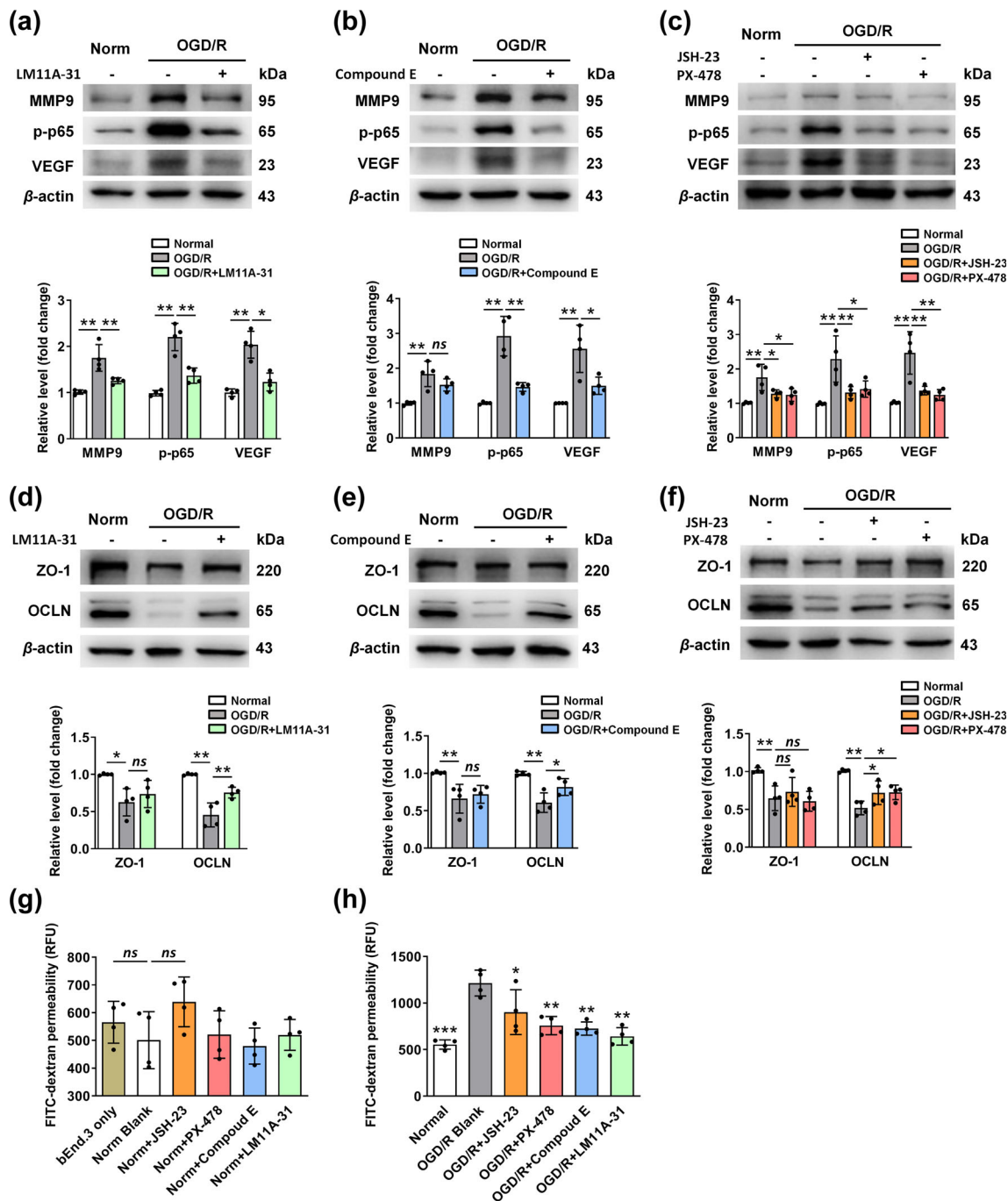
FIGURE 8 Inhibition of p75[NTR], NF-κB p–p-65, or HIF-1α protects the BBB integrity after OGD reoxygenation. (a–c) Western blot analysis and quantification of MMP-9, VEGF, and p-p65 expression in astrocytes treated with (a) LM11A-31, a p75[NTR] inhibitor, (b) compound E, a γ-secretase inhibitor, (c) JSH-23, a p-p65 inhibitor and/or PX-478, a HIF-1α inhibitor. (d–f) Western blot analysis and quantification of ZO-1 and occludin expression in bEnd.3 endothelial cells after OGD/R when added conditioned medium from astrocytes which were treated with (d) LM11A-31, (e) compound E, (f) JSH-23 and/or PX-478 during the OGD/R processes. (g) The in vitro BBB integrity measured by FITC-dextran (70 kDa) across the BBB in different treatment groups in normal O_2 conditions. (h) The in vitro BBB permeability to FITC-dextran (70 kDa) when exposed to different inhibitors during the OGD/R. data are expressed as the means ± SD. $N = 4$.*$p < .05$; **$p < .01$; ***$p < .001$; ns, not significant. Norm, normal O_2 conditions; OGD/R, oxygen and glucose deprivation/reoxygenation; OCLN, occludin; ZO-1, zonula occludens-1

3.7 | p75[NTR] regulates OGD-induced BBB disruption via NF-κB and HIF-1a signals *in vitro*

To further verify the function of astroglial p75[NTR] in the BBB integrity during the OGD/R, we treated primary astrocytes with LM11A-31

(blocking the ligand binding site of p75[NTR] (Simmons, 2017) and the compound E (the γ-secretase inhibitor, blocking the cleavage of ICD of p75[NTR]) (Forsyth et al., 2014; Le Moan et al., 2011; Schachtrup et al., 2015) to pharmacologically block signal transduction of p75[NTR]. Please note, both LM11A-31 and compound E did not affect the
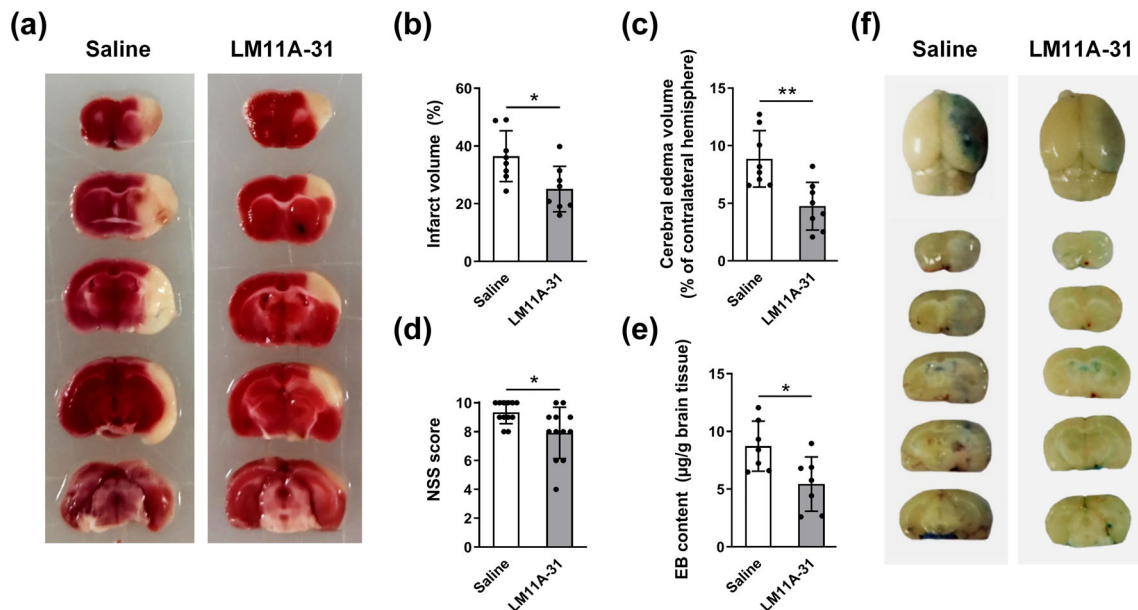
FIGURE 9 The p75^NTR inhibitor LM11A-31 ameliorates stroke-induced brain ischemia injury, and improves neurological functions after ischemic stroke. (a) Representative TTC staining of mice brains treated with saline or LM11A-31 by intravenous injection. (b) Quantitative analysis of infarct volume. $N = 8$. (c) Quantitative analysis of relative edema volumes by measuring ischemic hemispheric enlargements. $N = 8$. (d) Neurological severity scores. $N = 12$. (e) Quantitative analysis of EB content in ischemic hemispheres. $N = 7$. (f) Representative EB staining of mice brains. Data are expressed as the mean ± SD. $*p < .05$; $**p < .01$; $***p < .001$

integrity of the in vitro BBB model in normal conditions (Figure 8g), indicating no cytotoxicity of the drugs to the BBB. We found that LM11A-31 (Figure 8a) and compound E (Figure 8b) both hampered the increase of p-p65, MMP9 and VEGF proteins (LM11A-31: p-p65, MMP9, and VEGF, $**p < .01$, $**p < .01$, $**p < .01$, respectively; Compound E: MMP9 not significant $p = .1696$, p-p65 $**p < .01$, VEGF $*p < .05$) in astrocytes after exposure to OGD/R (Figure 8a,b). As well, CM from LM11A-31-treated astrocytes prevented downregulation of OCLN ($**p < .01$) in bEnd.3 endothelial cells during the OGD/R processes and partially preserved ZO-1 expression (not significant, $p = .4245$) (Figure 8d). Similarly, CM from compound E treated astrocytes significantly prevented the decline of OCLN protein expression ($*p < .05$) during the OGD/R (Figure 8e). As expected, following OGD/R, LM11A-31 ($**p < .01$) or compound E ($**p < .01$) both significantly protected the integrity of the in vitro BBB (Blank: 1214.58 ± 138.86; LM11A-31: 642.22 ± 93.87; compound E: 725.57 ± 71.16) (Figure 8h). Thus, our results indicate that inhibition of astroglial p75^NTR is beneficial for the BBB integrity after OGD/R.

p75^NTR was reported to activate NF-κB signaling (Caporali et al., 2015) and p75^NTR can directly interact with the E3 RING ubiquitin ligase (Siah2) which regulates HIF-1α degradation, thus, stabilizes HIF-1α proteins and upregulates VEGF expression under the HIF-1α promotor in hypoxia conditions (Le Moan et al., 2011). Therefore, we next blocked the NF-κB signaling and HIF-1α signaling separately by using their selective inhibitors, JSH-23 and PX-478, respectively. In astrocytes, JSH-23 and PX-478 both attenuated upregulation of p-p65 (JSH-23: $**p < .01$; PX-478: $*p < .05$), MMP9 (JSH-23: $*p < .05$; PX-478: $*p < .05$), and VEGF (JSH-23: $**p < .01$;

PX-478: $**p < .01$) (Figure 8c), strongly suggesting NF-κB and HIF-1α mediate MMP9 and VEGF expression in astrocytes under hypoxia. Additionally, CM from JSH-23 treated or PX-478 treated astrocytes inhibited downregulation of OCLN ($*p < .05$) in bEnd.3 cells exposed to OGD/R (Figure 8f), but not for the decrease of ZO-1 (JSH-23: $p = .4412$; PX-478: $p = .5613$) (Figure 8f). Nevertheless, both JSH-23 and PX-478 protected the integrity of the in vitro BBB (Blank: 1214.58 ± 138.86; JSH-23: 901.97 ± 240.60; PX-478: 757.81 ± 98.17) following OGD/R (Figure 8h). Therefore, our results suggest that astroglial p75^NTR causes BBB disruption after ischemia injury via NF-κB and HIF-1α signaling pathways.

3.8 | LM11A-31 improve ischemic stroke-induced outcomes

Considering the importance of p75^NTR in BBB breakdown, we investigated the potential application of p75^NTR as a therapeutic target of ischemic stroke. The p75^NTR inhibitor, LM11A-31 is a small molecule with high BBB permeability for which the phase 2 clinical trials in AD patients has been finished (Mufson et al., 2019; Patnaik et al., 2020). Thus, we utilized LM11A-31 in an attempt to reduce brain ischemic injury. Compared to vehicle (saline), tail vein administration of LM11A-31 (50 mg/kg) immediately after MCAO operation significantly decreased the volumes of infarct region (Saline: 36.46 ± 8.81%; LM11A-31: 25.11 ± 7.89%; $*p < .05$) 24 h after stroke (Figure 9a,b) and reduced ischemia-induced brain edema (Saline: 8.86 ± 2.49%; LM11A-31: 5.23 ± 2.54%; $**p < .01$) (Figure 9c), as well as the EB

extravasation into the parenchyma (Saline: 8.73 ± 2.17 μg/g; LM11A-31: 4.76 ± 2.07 μg/g; *p < .05) (Figure 9e,f). Furthermore, LM11A-31 administration significantly decreased NSS (Saline: 9.33 ± 0.78 ; LM11A-31: 7.92 ± 1.78; *p < .05) after brain ischemia injury (Figure 9d). Together, these results strongly implicate p75^{NTR} as a potential therapeutic target of ischemic stroke by preventing BBB breakdown and improving functional outcomes.

4 | DISCUSSION

p75^{NTR} expression in the brain has been demonstrated to be provoked in different cell types (e.g., neurons, astrocytes, and endothelial cells) by a variety of pathological insults such as ischemic stroke (Irmady et al., 2014; Mufson et al., 2019), though the focus was mainly on its functions to induce neuronal apoptosis. In the current study, we also observed that p75^{NTR} was already upregulated in the infarct-affected area at 1 hpi in a mouse MCAO model of ischemic stroke. We further showed that the enhanced p75^{NTR} expression was first detected in neurons and subsequently in a subset of astrocytes and endothelial cells at least at 8 hpi, suggesting contributions of non-neuronal p75^{NTR} to the pathological progression in ischemic stroke. Since astrocytes and endothelial cells are primary components of the BBB, our results strongly suggest p75^{NTR} might play important roles in regulating BBB functions after ischemic stroke. Indeed, a recently study showed ischemia reperfusion injury upregulated p75^{NTR} expression in endothelials in neonatal mice brain and the upregulated p75^{NTR} could induce endothelial cell death and disruption of tight junction proteins after OGD/R (Kuo et al., 2019). However, the function of astrocytic p75^{NTR} remains elusive. Utilizing cell-specific p75^{NTR} knockdown strategies in astrocytes in vivo and in vitro, in the present study we demonstrated that astrocytic p75NTR contributed to the disruption of the BBB to exacerbate brain ischemic injury. To our knowledge, this was the first study to characterize the role of astrocytic p75^{NTR} in ischemic brain injury.

In line with previous studies using p75$^{NTR-/-}$ mice, we observed improved outcomes such as reduced infarct volume and neurological scores in p75$^{NTR+/-}$ mice after MCAO. Moreover, the BBB integrity was also better preserved in the p75$^{NTR+/-}$ mice after ischemic injury. To assess the contribution of astrocytic p75^{NTR} to the BBB disruption, we specifically knockdown the p75^{NTR} in astrocytes by an AAV-mediated shRNA approach (p75^{NTR} cKD). Consistent with the results of genetic p75^{NTR} knockdown in p75$^{NTR+/-}$ mice, cKD of astrocytic p75^{NTR} also improved the BBB function as well as other outcomes after ischemic stroke, however, to a less extent. These results agreed with previous studies that the elevated p75^{NTR} from other cellular sources such as neurons and endothelial cells also contribute to the pathology of ischemic stroke. For example, studies in the retinal ischemia reported that endothelial p75^{NTR} increasing blood-retinal barrier permeability by inducing endothelial cell apoptosis via activation of JNK,p38 MAPK and cleaved-PARP signaling pathways or by reducing tight junction protein expression and redistribution in the cell wall via RhoA-F-actin pathway (Elshaer et al., 2019; Shanab et al., 2015).

Recently, Kuo et al. even showed that p75^{NTR} caused bEnd.3 endothelial cells apoptosis and tight junction degradation under OGD and reoxygen injury (Kuo et al., 2019). In addition, upregulated p75^{NTR} in neurons has been reported to cause neuronal apoptosis after stroke (Irmady et al., 2014; Jover et al., 2002; Park et al., 2000). However, astrocytic p75^{NTR} was reported to not induce apoptosis but to cause astrocyte activation after brain injuries (Schachtrup et al., 2015). Likewise, our results showed that astrocytic p75^{NTR} knockdown reduced GFAP expression in the infarct-affected area after MCAO. Moreover, p75^{NTR} siRNA or p75^{NTR} overexpression did not have a significant effect on cell viability of astrocytes when exposed to 4-h OGD/R in vitro. Taken together, these results suggest that p75^{NTR} upregulation induced astrocyte activation rather than apoptosis to exacerbate BBB disruption after ischemic stroke.

It is known that activated astrocytes could secrete MMPs (e.g., MMP-9) and cytokines (e.g., VEGF) causing degradation of TJ proteins, thereby destroying BBB integrity (Argaw et al., 2012; Li et al., 2014; Zhang et al., 2018). We also found that knockdown of astrocytic p75^{NTR} decreased MMP-9 and VEGF expression, reducing the degradation of TJ proteins (e.g. ZO-1 and OCLN). Consistent with other studies (Le Moan et al., 2011; Schachtrup et al., 2015), we could show that cleavage of p75^{NTR} by γ-secretase was essential for its functioningin regulating MMP9 and VEGF expression. Furthermore, we identified NF-κB signaling was involved in the downstream functions of astrocytic p75^{NTR}. NF-κB is known to regulate glial inflammatory response (Frakes et al., 2014; Xu et al., 2017; Zaghloul et al., 2020), therefore astrocytic p75^{NTR} might contribute to not only BBB breakdown but also augmented neuroinflammation, synergistically promoting cellular response (e.g., leukocyte infiltration and microglia activation), brain edema/damage as well as impaired neurological functions after stroke. On the other hand, although p75^{NTR} was shown to induce endothelial cell death, we only observed a subset of endothelial cells increasing p75^{NTR} expression upon ischemic injury and the proportion of these p75^{NTR}-expressing endothelial cells was rather maintained at about 30%. Moreover, many studies suggested ischemic injuries induced very limited, irrespective the p75^{NTR} expression, endothelial cell loss in vivo. For example, Krueger et al. (Krueger et al., 2015) showed only less than 2% of blood vessels lost endothelial cells in the infarct core area and almost no blood vessels lost endothelial cells in the penumbra 24 h after MCAO. Another study reported that only 10% of all endothelial cells were TUNEL-positive at 3 days after MCAO in rats (Zuo et al., 2018). Therefore, we might suggest in the area without enhanced endothelial p75^{NTR} expression astrocytic p75^{NTR} significantly contributes to the disrupted tight junctions in terms of triggering cytokines and MMPs released from activated astrocytes, which was suggested as the major causes of BBB leakage after ischemic stroke in previous studies (Bernardo-Castro et al., 2020; Gao et al., 2020; Jiang et al., 2018). Nevertheless, further studies are required to investigate the detailed mechanisms of p75^{NTR} in regulating functions and interactions of astrocytes and endothelial cells in ischemic stroke.

Last but not least, p75^{NTR} may be a potential pharmaceutical target for ischemic stroke. The p75^{NTR} inhibitor, LM11A-31, is a non-

peptide small molecule which has structural and chemical features similar to the NGF loop 1β-turn domain and can cross the BBB (Massa et al., 2006; Nguyen et al., 2014). Administration of 50 mg/kg LM11A-31, significantly reduced BBB permeability, brain edema, infarct volumes, and further alleviated neurological deficits after stroke, suggesting that LM11A-31 was neuroprotective after ischemic stroke. The protective effect of LM11A-31 was partially due to the inhibition of astrocytic p75^{NTR}, but we could not exclude the contribution of inhibitory effect of LM11A-31 on the neuronal and endothelial p75^{NTR}. Thus, further investigation on the role of neuronal or endothelial p75^{NTR} is required. Nevertheless, because oral administration of LM11A-31 has finished phase 2 clinical trials in AD patients (results currently has not been reported) and did not show significant cytotoxicity or cardiotoxicity in phase 1 clinical trials (Mufson et al., 2019; Patnaik et al., 2020), long term preventive administration of LM11A-31 is possible. So, our findings suggested that LM11A-31 might be a potential preventive or therapeutic drug for ischemic stroke.

In conclusion, our results provided novel insight into the role of astrocytic p75^{NTR} in BBB disruption during acute cerebral ischemia. Knockdown of astrocytic p75^{NTR} ameliorated BBB leakage through inhibition of the NF-κB p-65 and HIF-1α signaling pathways, and preserved tight junctions by reducing astrocyte-derived MMP-9 and VEGF. The protected BBB inhibited leukocyte infiltration and microglia activation, thus may alleviate brain tissue damage, leading to an overall functional improvement after ischemic stroke. In addition, the p75^{NTR} inhibitor, LM11A-31, significantly mitigated BBB leakage and cerebral infarction, and thereby protected neurological functions after stroke. Overall, these results suggested that astrocytic p75^{NTR} was critical in BBB disruption, and p75^{NTR} might be a potential therapeutic target for treatment of ischemic stroke. Because BBB disruption is an important contributor to several inflammatory brain disorders, the findings of this study may be applied to other disease processes including, but not limited to ischemic stroke.

CONFLICT OF INTEREST

The authors declared that no competing interest exists.

AUTHOR CONTRIBUTIONS

Xiaoying Qin participated in experiment design, performed MCAO operation, data collection of Western blot and IHC experiments, statistical analyses, and interpretation of data and drafted the manuscript. Jianing Wang participated in cell culture experiment. Shujian Chen contributed to AAV injection. Gang Liu assisted in data collection of IHC experiments. Chaoran Wu contributed to MACS experiment. Qunyu Lv and Xinran He contributed to assessment of NSS scores. Xianshu Bai contributed to the establishment of the co-culture system, and manuscript preparation. Wenhui Huang contributed to conceptualization and design of the study, as well as manuscript preparation and revision. Hong Liao conceptualized the study, organized and supervised experiments, and revised the manuscript.

DATA AVAILABILITY STATEMENT

Data availability statement The data that support the findings of this study are available from the corresponding author upon reasonable request.

ORCID

Xiaoying Qin https://orcid.org/0000-0001-9641-4256
Jianing Wang https://orcid.org/0000-0002-3563-5714
Qunyu Lv https://orcid.org/0000-0002-1608-2093
Xianshu Bai https://orcid.org/0000-0002-4758-1645
Wenhui Huang https://orcid.org/0000-0001-9865-0375
Hong Liao https://orcid.org/0000-0002-1010-5936

REFERENCES

Abdullahi, W., Tripathi, D., & Ronaldson, P. T. (2018). Blood-brain barrier dysfunction in ischemic stroke: Targeting tight junctions and transporters for vascular protection. *American Journal of Physiology. Cell Physiology, 315*(3), C343–C356. https://doi.org/10.1152/ajpcell.00095.2018

András, I. E., Deli, M. A., Veszelka, S., Hayashi, K., Hennig, B., & Toborek, M. (2007). The NMDA and AMPA/KA receptors are involved in glutamate-induced alterations of occludin expression and phosphorylation in brain endothelial cells. *Journal of Cerebral Blood Flow and Metabolism, 27*(8), 1431–1443. https://doi.org/10.1038/sj.jcbfm.9600445

Andsberg, G., Kokaia, Z., & Lindvall, O. (2001). Upregulation of p75 neurotrophin receptor after stroke in mice does not contribute to differential vulnerability of striatal neurons. *Experimental Neurology, 169*(2), 351–363. https://doi.org/10.1006/exnr.2001.7646

Angelo, M. F., Aviles-Reyes, R. X., Villarreal, A., Barker, P., Reines, A. G., & Ramos, A. J. (2009). p75 NTR expression is induced in isolated neurons of the penumbra after ischemia by cortical devascularization. *Journal of Neuroscience Research, 87*(8), 1892–1903. https://doi.org/10.1002/jnr.21993

Argaw, A. T., Asp, L., Zhang, J., Navrazhina, K., Pham, T., Mariani, J. N., Mahase, S., Dutta, D. J., Seto, J., Kramer, E. G., Ferrara, N., Sofroniew, M. V., & John, G. R. (2012). Astrocyte-derived VEGF-A drives blood-brain barrier disruption in CNS inflammatory disease. *The Journal of clinical investigation, 122*(7), 2454–2468. https://doi.org/10.1172/JCI60842

Bake, S., Okoreeh, A., Khosravian, H., & Sohrabji, F. (2019). Insulin-like growth factor (IGF)-1 treatment stabilizes the microvascular cytoskeleton under ischemic conditions. *Experimental Neurology, 311*, 162–172. https://doi.org/10.1016/j.expneurol.2018.09.016

Barcelona, P. F., Sitaras, N., Galan, A., Esquiva, G., Jmaeff, S., Jian, Y., Sarunic, M. V., Cuenca, N., Sapieha, P., & Saragovi, H. U. (2016). p75NTR and its ligand ProNGF activate paracrine mechanisms etiological to the vascular, inflammatory, and neurodegenerative pathologies of diabetic retinopathy. *The Journal of Neuroscience, 36*(34), 8826–8841. https://doi.org/10.1523/JNEUROSCI.4278-15.2016

Begum, G., Song, S., Wang, S., Zhao, H., Bhuiyan, M., Li, E., Nepomuceno, R., Ye, Q., Sun, M., Calderon, M. J., Stolz, D. B., St Croix, C., Watkins, S. C., Chen, Y., He, P., Shull, G. E., & Sun, D. (2018). Selective knockout of astrocytic Na+ /H+ exchanger isoform 1 reduces astrogliosis, BBB damage, infarction, and improves neurological function after ischemic stroke. *Glia*, 66(1), 126–144. https://doi.org/10.1002/glia.23232

Bernardo-Castro, S., Sousa, J. A., Brás, A., Cecília, C., Rodrigues, B., Almendra, L., Machado, C., Santo, G., Silva, F., Ferreira, L., Santana, I., & Sargento-Freitas, J. (2020). Pathophysiology of blood-brain barrier permeability throughout the different stages of ischemic stroke and its implication on hemorrhagic transformation and recovery. *Frontiers in Neurology*, 11, 594672. https://doi.org/10.3389/fneur.2020.594672

Bernstein, D. L., Zuluaga-Ramirez, V., Gajghate, S., Reichenbach, N. L., Polyak, B., Persidsky, Y., & Rom, S. (2020). miR-98 reduces endothelial dysfunction by protecting blood-brain barrier (BBB) and improves neurological outcomes in mouse ischemia/reperfusion stroke model. *Journal of Cerebral Blood Flow and Metabolism*, 40(10), 1953–1965. https://doi.org/10.1177/0271678X19882264

Caporali, R., Todoerti, M., Scirè, C. A., Montecucco, C., & Cutolo, M. (2015). Oral low-dose glucocorticoids should be included in any recommendation for the use of non-biologic and biologic disease-modifying antirheumatic drugs in the treatment of rheumatoid arthritis. *Neuroimmunomodulation*, 22(1–2), 104–111. https://doi.org/10.1159/000362730

Caracciolo, L., Marosi, M., Mazzitelli, J., Latifi, S., Sano, Y., Galvan, L., Kawaguchi, R., Holley, S., Levine, M. S., Coppola, G., Portera-Cailliau, C., Silva, A. J., & Carmichael, S. T. (2018). CREB controls cortical circuit plasticity and functional recovery after stroke. *Nature Communications*, 9(1), 2250. https://doi.org/10.1038/s41467-018-04445-9

Chen, A. Q., Fang, Z., Chen, X. L., Yang, S., Zhou, Y. F., Mao, L., Xia, Y. P., Jin, H. J., Li, Y. N., You, M. F., Wang, X. X., Lei, H., He, Q. W., & Hu, B. (2019). Microglia-derived TNF-α mediates endothelial necroptosis aggravating blood brain-barrier disruption after ischemic stroke. *Cell Death & Disease*, 10(7), 487. https://doi.org/10.1038/s41419-019-1716-9

Cheng, I., Jin, L., Rose, L. C., & Deppmann, C. D. (2018). Temporally restricted death and the role of p75NTR as a survival receptor in the developing sensory nervous system. *Developmental Neurobiology*, 78(7), 701–717. https://doi.org/10.1002/dneu.22591

Elshaer, S. L., Alwhaibi, A., Mohamed, R., Lemtalsi, T., Coucha, M., Longo, F. M., & El-Remessy, A. B. (2019). Modulation of the p75 neurotrophin receptor using LM11A-31 prevents diabetes-induced retinal vascular permeability in mice via inhibition of inflammation and the RhoA kinase pathway. *Diabetologia*, 62(8), 1488–1500. https://doi.org/10.1007/s00125-019-4885-2

Fann, D. Y., Lim, Y. A., Cheng, Y. L., Lok, K. Z., Chunduri, P., Baik, S. H., Drummond, G. R., Dheen, S. T., Sobey, C. G., Jo, D. G., Chen, C. L., & Arumugam, T. V. (2018). Evidence that NF-κB and MAPK signaling promotes NLRP Inflammasome activation in neurons following ischemic stroke. *Molecular Neurobiology*, 55(2), 1082–1096. https://doi.org/10.1007/s12035-017-0394-9

Fernandez Esmerats, J., Villa-Roel, N., Kumar, S., Gu, L., Salim, M. T., Ohh, M., ... Jo, H. (2019). Disturbed flow increases UBE2C (ubiquitin E2 ligase C) via loss of miR-483-3p, inducing aortic valve calcification by the pVHL (von Hippel-Lindau protein) and HIF-1α (hypoxia-inducible factor-1α) pathway in endothelial cells. *Arteriosclerosis, Thrombosis, and Vascular Biology*, 39(3), 467–481. https://doi.org/10.1161/ATVBAHA.118.312233

Filchenko, I., Blochet, C., Buscemi, L., Price, M., Badaut, J., & Hirt, L. (2020). Caveolin-1 regulates perivascular aquaporin-4 expression after cerebral ischemia. *Frontiers in Cell and Development Biology*, 8, 371. https://doi.org/10.3389/fcell.2020.00371

Flierl, M. A., Stahel, P. F., Beauchamp, K. M., Morgan, S. J., Smith, W. R., & Shohami, E. (2009). Mouse closed head injury model induced by a weight-drop device. *Nature Protocols*, 4(9), 1328–1337. https://doi.org/10.1038/nprot.2009.148

Forsyth, P. A., Krishna, N., Lawn, S., Valadez, J. G., Qu, X., Fenstermacher, D. A., Potthast, L., Chinnaiyan, P., Gibney, G. T., Zeinieh, M., Barker, P. A, Carter, B. D., Cooper, M. K., & Kenchappa, R. S. (2014). p75 neurotrophin receptor cleavage by α- and γ-secretases is required for neurotrophin-mediated proliferation of brain tumor-initiating cells. *The Journal of Biological Chemistry*, 289(12), 8067–8085. https://doi.org/10.1074/jbc.M113.513762

Frakes, A. E., Ferraiuolo, L., Haidet-Phillips, A. M., Schmelzer, L., Braun, L., Miranda, C. J., Ladner, K. J., Bevan, A. K., Foust, K. D., Godbout, J. P., Popovich, P. G., Guttridge, D. C., & Kaspar, B. K. (2014). Microglia induce motor neuron death via the classical NF-κB pathway in amyotrophic lateral sclerosis. *Neuron*, 81(5), 1009–1023. https://doi.org/10.1016/j.neuron.2014.01.013

Gao, L., Song, Z., Mi, J., Hou, P., Xie, C., Shi, J., Li, Y., & Manaenko, A. (2020). The effects and underlying mechanisms of cell therapy on blood-brain barrier integrity after ischemic stroke. *Current Neuropharmacology*, 18(12), 1213–1226. https://doi.org/10.2174/1570159X18666200914162013

Harari, O. A., & Liao, J. K. (2010). NF-κB and innate immunity in ischemic stroke. *Annals of the New York Academy of Sciences*, 1207, 32–40. https://doi.org/10.1111/j.1749-6632.2010.05735.x

Hayakawa, K., Esposito, E., Wang, X., Terasaki, Y., Liu, Y., Xing, C., Ji, X., & Lo, E. H. (2016). Transfer of mitochondria from astrocytes to neurons after stroke. *Nature*, 535(7613), 551–555. https://doi.org/10.1038/nature18928

Holt, L. M, Stoyanof, S. T., & Olsen, M. L. (2019). Magnetic cell sorting for in vivo and in vitro astrocyte, neuron, and microglia analysis. *Current protocols in neuroscience*, 88(1), e71. https://doi.org/10.1002/cpns.71

Howell, J. A., & Bidwell, G. L. (2020). Targeting the NF-κB pathway for therapy of ischemic stroke. *Therapeutic Delivery*, 11(2), 113–123. https://doi.org/10.4155/tde-2019-0075

Huang, W., Bai, X., Meyer, E., & Scheller, A. (2020). Acute brain injuries trigger microglia as an additional source of the proteoglycan NG2. *Acta Neuropathologica Communications*, 8(1), 146. https://doi.org/10.1186/s40478-020-01016-2

Irmady, K., Jackman, K. A., Padow, V. A., Shahani, N., Martin, L. A., Cerchietti, L., Unsicker, K., Iadecola, C., & Hempstead, B. L. (2014). Mir-592 regulates the induction and cell death-promoting activity of p75NTR in neuronal ischemic injury. *The Journal of Neuroscience*, 34(9), 3419–3428. https://doi.org/10.1523/JNEUROSCI.1982-13.2014

Jiang, X., Andjelkovic, A. V., Zhu, L., Yang, T., Bennett, M. V. L., Chen, J., Keep, R. F., & Shi, Y. (2018). Blood-brain barrier dysfunction and recovery after ischemic stroke. *Progress in Neurobiology*, 163-164, 144–171. https://doi.org/10.1016/j.pneurobio.2017.10.001

Jiao, H., Wang, Z., Liu, Y., Wang, P., & Xue, Y. (2011). Specific role of tight junction proteins claudin-5, occludin, and ZO-1 of the blood-brain barrier in a focal cerebral ischemic insult. *Journal of Molecular Neuroscience*, 44(2), 130–139. https://doi.org/10.1007/s12031-011-9496-4

Jover, T., Tanaka, H., Calderone, A., Oguro, K., Bennett, M. V., Etgen, A. M., & Zukin, R. S. (2002). Estrogen protects against global ischemia-induced neuronal death and prevents activation of apoptotic signaling cascades in the hippocampal CA1. *The Journal of Neuroscience*, 22(6), 2115–2124. https://doi.org/10.1523/JNEUROSCI.22-06-02115.2002

Kassner, A., & Merali, Z. (2015). Assessment of blood-brain barrier disruption in stroke. *Stroke*, 46(11), 3310–3315. https://doi.org/10.1161/STROKEAHA.115.008861

Knowland, D., Arac, A., Sekiguchi, K. J., Hsu, M., Lutz, S. E., Perrino, J., Steinberg, G. K., Barres, B. A., Nimmerjahn, A., & Agalliu, D. (2014). Stepwise recruitment of transcellular and paracellular pathways

underlies blood-brain barrier breakdown in stroke. *Neuron*, 82(3), 603–617. https://doi.org/10.1016/j.neuron.2014.03.003

Knowles, J. K., Simmons, D. A., Nguyen, T. V., Vander Griend, L., Xie, Y., Zhang, H., Yang, T., Pollak, J., Chang, T., Arancio, O., Buckwalter, M. S., Wyss-Coray, T., Massa, S. M., & Longo, F. M. (2013). Small molecule p75NTR ligand prevents cognitive deficits and neurite degeneration in an Alzheimer's mouse model. *Neurobiology of Aging*, 34(8), 2052–2063. https://doi.org/10.1016/j.neurobiolaging.2013.02.015

Krueger, M., Bechmann, I., Immig, K., Reichenbach, A., Härtig, W., & Michalski, D. (2015). Blood-brain barrier breakdown involves four distinct stages of vascular damage in various models of experimental focal cerebral ischemia. *Journal of Cerebral Blood Flow and Metabolism*, 35(2), 292–303. https://doi.org/10.1038/jcbfm.2014.199

Krueger, M., Mages, B., Hobusch, C., & Michalski, D. (2019). Endothelial edema precedes blood-brain barrier breakdown in early time points after experimental focal cerebral ischemia. *Acta Neuropathologica Communications*, 7(1), 17. https://doi.org/10.1186/s40478-019-0671-0

Kuo, M. H., Lee, H. F., Tu, Y. F., Lin, L. H., Cheng, Y. Y., & Lee, H. T. (2019). Astaxanthin ameliorates ischemic-hypoxic-induced neurotrophin receptor p75 Upregulation in the endothelial cells of neonatal mouse brains. *International Journal of Molecular Sciences*, 20(24), 6168. https://doi.org/10.3390/ijms20246168

Le Moan, N., Houslay, D. M., Christian, F., Houslay, M. D., & Akassoglou, K. (2011). Oxygen-dependent cleavage of the p75 neurotrophin receptor triggers stabilization of HIF-1α. *Molecular Cell*, 44(3), 476–490. https://doi.org/10.1016/j.molcel.2011.08.033

Lebrun-Julien, F., Bertrand, M. J., De Backer, O., Stellwagen, D., Morales, C. R., Di Polo, A., & Barker, P. A. (2010). ProNGF induces TNFalpha-dependent death of retinal ganglion cells through a p75NTR non-cell-autonomous signaling pathway. *Proceedings of the National Academy of Sciences of the United States of America*, 107(8), 3817–3822. https://doi.org/10.1073/pnas.0909276107

Li, Y., Zhu, Z. Y., Huang, T. T., Zhou, Y. X., Wang, X., Yang, L. Q., Chen, Z. A., Yu, W. F.,, & Li, P. Y. (2018). The peripheral immune response after stroke-a double edge sword for blood-brain barrier integrity. *CNS Neuroscience & Therapeutics*, 24(12), 1115–1128. https://doi.org/10.1111/cns.13081

Li, Y. N., Pan, R., Qin, X. J., Yang, W. L., Qi, Z., Liu, W., & Liu, K. J. (2014). Ischemic neurons activate astrocytes to disrupt endothelial barrier via increasing VEGF expression. *Journal of Neurochemistry*, 129(1), 120–129. https://doi.org/10.1111/jnc.12611

Liang, H., Matei, N., McBride, D. W., Xu, Y., Tang, J., Luo, B., & Zhang, J. H. (2020). Activation of TGR5 protects blood brain barrier via the BRCA1/Sirt1 pathway after middle cerebral artery occlusion in rats. *Journal of Biomedical Science*, 27(1), 61. https://doi.org/10.1186/s12929-020-00656-9

Lin, Y., Zhang, J. C., Fu, J., Chen, F., Wang, J., Wu, Z. L., & Yuan, S. Y. (2013). Hyperforin attenuates brain damage induced by transient middle cerebral artery occlusion (MCAO) in rats via inhibition of TRPC6 channels degradation. *Journal of Cerebral Blood Flow and Metabolism*, 33(2), 253–262. https://doi.org/10.1038/jcbfm.2012.164

Liu, D., Yang, L., Liu, P., Ji, X., Qi, X., Wang, Z., Chi, T., & Zou, L. (2022). Sigma-1 receptor activation alleviates blood-brain barrier disruption post cerebral ischemia stroke by stimulating the GDNF-GFRα1-RET pathway. *Experimental Neurology*, 347, 113867. https://doi.org/10.1016/j.expneurol.2021.113867

Lo, A. C., Chen, A. Y., Hung, V. K., Yaw, L. P., Fung, M. K., Ho, M. C., Tsang, M. C., Chung, S. S., & Chung, S. K. (2005). Endothelin-1 overexpression leads to further water accumulation and brain edema after middle cerebral artery occlusion via aquaporin 4 expression in astrocytic end-feet. *Journal of Cerebral Blood Flow and Metabolism*, 25(8), 998–1011. https://doi.org/10.1038/sj.jcbfm.9600108

Ma, F., Sun, P., Zhang, X., Hamblin, M. H., & Yin, K. J. (2020). Endothelium-targeted deletion of the miR-15a/16-1 cluster ameliorates blood-brain

barrier dysfunction in ischemic stroke. *Science Signaling*, 13(626), eaay5658. https://doi.org/10.1126/scisignal.aay5686

Massa, S. M., Xie, Y., Yang, T., Harrington, A. W., Kim, M. L., Yoon, S. O., Kraemer, R., Moore, L. A., Hempstead, B. L., & Longo, F. M. (2006). Small, nonpeptide p75NTR ligands induce survival signaling and inhibit proNGF-induced death. *The Journal of Neuroscience*, 26(20), 5288–5300. https://doi.org/10.1523/JNEUROSCI.3547-05.2006

Matsumoto, K., Nohara, Y., Soejima, H., Yonehara, T., Nakashima, N., & Kamouchi, M. (2020). Stroke prognostic scores and data-driven prediction of clinical outcomes after acute ischemic stroke. *Stroke*, 51(5), 1477–1483. https://doi.org/10.1161/STROKEAHA.119.027300

Michinaga, S., & Koyama, Y. (2019). Dual roles of astrocyte-derived factors in regulation of blood-brain barrier function after brain damage. *International Journal of Molecular Sciences*, 20(3), 571. https://doi.org/10.3390/ijms20030571

Morizawa, Y. M., Hirayama, Y., Ohno, N., Shibata, S., Shigetomi, E., Sui, Y., Nabekura, J., Sato, K., Okajima, F., Takebayashi, H., Okano, H., & Koizumi, S. (2017). Reactive astrocytes function as phagocytes after brain ischemia via ABCA1-mediated pathway. *Nature Communications*, 8(1), 28. https://doi.org/10.1038/s41467-017-00037-1

Mufson, E. J., Counts, S. E., Ginsberg, S. D., Mahady, L., Perez, S. E., Massa, S. M., Longo, F. M., & Ikonomovic, M. D. (2019). Nerve growth factor pathobiology during the progression of Alzheimer's disease. *Frontiers in Neuroscience*, 13, 533. https://doi.org/10.3389/fnins.2019.00533

Mysona, B. A., Al-Gayyar, M. M., Matragoon, S., Abdelsaid, M. A., El-Azab, M. F., Saragovi, H. U., & El-Remessy, A. B. (2013). Modulation of p75(NTR) prevents diabetes- and proNGF-induced retinal inflammation and blood-retina barrier breakdown in mice and rats. *Diabetologia*, 56(10), 2329–2339. https://doi.org/10.1007/s00125-013-2998-6

Nguyen, T. V., Shen, L., Vander Griend, L., Quach, L. N., Belichenko, N. P., Saw, N., Shamloo, M., Wyss-Coray, T., Massa, S. M., & Longo, F. M. (2014). Small molecule p75NTR ligands reduce pathological phosphorylation and misfolding of tau, inflammatory changes, cholinergic degeneration, and cognitive deficits in AβPP(L/S) transgenic mice. *Journal of Alzheimer's Disease*, 42(2), 459–483. https://doi.org/10.3233/JAD-140036

Oderfeld-Nowak, B., Orzyłowska-Sliwińska, O., Sołtys, Z., Zaremba, M., Januszewski, S., Janeczko, K., & Mossakowski, M. (2003). Concomitant up-regulation of astroglial high and low affinity nerve growth factor receptors in the CA1 hippocampal area following global transient cerebral ischemia in rat. *Neuroscience*, 120(1), 31–40. https://doi.org/10.1016/s0306-4522(03)00289-6

Pan, S., Hu, Y., Hu, M., Xu, Y., Chen, M., Du, C., Cui, J., Zheng, P., Lai, J., Zhang, Y., Bai, J., Jiang, P., Zhu, J., He, Y., & Wang, J. (2020). S100A8 facilitates cholangiocarcinoma metastasis via upregulation of VEGF through TLR4/NF-κB pathway activation. *International Journal of Oncology*, 56(1), 101–112. https://doi.org/10.3892/ijo.2019.4907

Park, J. A., Lee, J. Y., Sato, T. A., & Koh, J. Y. (2000). Co-induction of p75NTR and p75NTR-associated death executor in neurons after zinc exposure in cortical culture or transient ischemia in the rat. *The Journal of Neuroscience*, 20(24), 9096–9103. https://doi.org/10.1523/JNEUROSCI.20-24-09096.2000

Patabendige, A., Singh, A., Jenkins, S., Sen, J., & Chen, R. (2021). Astrocyte activation in neurovascular damage and repair following ischaemic stroke. *International Journal of Molecular Sciences*, 22(8), 4280. https://doi.org/10.3390/ijms22084280

Patnaik, A., Zagrebelsky, M., Korte, M., & Holz, A. (2020). Signaling via the p75 neurotrophin receptor facilitates amyloid-β-induced dendritic spine pathology. *Scientific Reports*, 10(1), 13322. https://doi.org/10.1038/s41598-020-70153-4

Peng, L., Zhou, Y., Jiang, N., Wang, T., Zhu, J., Chen, Y., Li, L., Zhang, J., Yu, S., & Zhao, Y. (2020). DJ-1 exerts anti-inflammatory effects and regulates NLRX1-TRAF6 via SHP-1 in stroke. *Journal of*

Neuroinflammation, 17(1), 81. https://doi.org/10.1186/s12974-020-01764-x

Pirson, F. A. V., van Oostenbrugge, R. J., van Zwam, W. H., Remmers, M. J. M., Dippel, D. W. J., van Es, A. C. G. M., ... Staals, J. (2020). Repeated endovascular thrombectomy in patients with acute ischemic stroke: Results from a nationwide multicenter database. *Stroke, 51*(2), 526–532. https://doi.org/10.1161/STROKEAHA.119.027525

Prakash, R., & Carmichael, S. T. (2015). Blood-brain barrier breakdown and neovascularization processes after stroke and traumatic brain injury. *Current Opinion in Neurology, 28*(6), 556–564. https://doi.org/10.1097/WCO.0000000000000248

Qin, W., Li, J., Zhu, R., Gao, S., Fan, J., Xia, M., Zhao, R. C., & Zhang, J. (2019). Melatonin protects blood-brain barrier integrity and permeability by inhibiting matrix metalloproteinase-9 via the NOTCH3/NF-κB pathway. *Aging (Albany NY), 11*(23), 11391–11415. https://doi.org/10.18632/aging.102537

Saadipour, K., Mañucat-Tan, N. B., Lim, Y., Keating, D. J., Smith, K. S., Zhong, J. H., Liao, H., Bobrovskaya, L., Wang, Y. J., Chao, M. V., & Zhou, X. F. (2018). p75 neurotrophin receptor interacts with and promotes BACE1 localization in endosomes aggravating amyloidogenesis. *Journal of Neurochemistry, 144*(3), 302–317. https://doi.org/10.1111/jnc.14206

Saha, R. N., & Pahan, K. (2006). Signals for the induction of nitric oxide synthase in astrocytes. *Neurochemistry International, 49*(2), 154–163. https://doi.org/10.1016/j.neuint.2006.04.007

Sandoval, K. E., & Witt, K. A. (2008). Blood-brain barrier tight junction permeability and ischemic stroke. *Neurobiology of Disease, 32*(2), 200–219. https://doi.org/10.1016/j.nbd.2008.08.005

Schachtrup, C., Ryu, J. K., Mammadzada, K., Khan, A. S., Carlton, P. M., Perez, A., Christian, F., Le Moan, N., Vagena, E., Baeza-Raja, B., Rafalski, V., Chan, J. P., Nitschke, R., Houslay, M. D., Ellisman, M. H., Wyss-Coray, T., Palop, J. J., & Akassoglou, K. (2015). Nuclear pore complex remodeling by p75(NTR) cleavage controls TGF-β signaling and astrocyte functions. *Nature Neuroscience, 18*(8), 1077–1080. https://doi.org/10.1038/nn.4054

Shan, Y., Tan, S., Lin, Y., Liao, S., Zhang, B., Chen, X., ... Lu, Z. (2019). The glucagon-like peptide-1 receptor agonist reduces inflammation and blood-brain barrier breakdown in an astrocyte-dependent manner in experimental stroke. *Journal of Neuroinflammation, 16*(1), 242. https://doi.org/10.1186/s12974-019-1638-6

Shanab, A. Y., Mysona, B. A., Matragoon, S., & El-Remessy, A. B. (2015). Silencing p75(NTR) prevents proNGF-induced endothelial cell death and development of acellular capillaries in rat retina. *Molecular Therapy Methods and Clinical Development, 2*, 15013. https://doi.org/10.1038/mtm.2015.13

Shi, J., Longo, F. M., & Massa, S. M. (2013). A small molecule p75(NTR) ligand protects neurogenesis after traumatic brain injury. *Stem Cells, 31*(11), 2561–2574. https://doi.org/10.1002/stem.1516

Shin, S. S., Dixon, C. E., Okonkwo, D. O., & Richardson, R. M. (2014). Neurostimulation for traumatic brain injury. *Journal of Neurosurgery, 121*(5), 1219–1231. https://doi.org/10.3171/2014.7.JNS131826

Sifat, A. E., Vaidya, B., & Abbruscato, T. J. (2017). Blood-brain barrier protection as a therapeutic strategy for acute ischemic stroke. *The AAPS Journal, 19*(4), 957–972. https://doi.org/10.1208/s12248-017-0091-7

Simmons, D. A. (2017). Modulating neurotrophin receptor signaling as a therapeutic strategy for Huntington's disease. *Journal of Huntingtons Diseases, 6*(4), 303–325. https://doi.org/10.3233/JHD-170275

Simmons, D. A., Belichenko, N. P., Ford, E. C., Semaan, S., Monbureau, M., Aiyaswamy, S., ... Longo, F. M. (2016). A small molecule p75NTR ligand normalizes signalling and reduces Huntington's disease phenotypes in R6/2 and BACHD mice. *Human Molecular Genetics, 25*(22), 4920–4938. https://doi.org/10.1093/hmg/ddw316

Sivandzade, F., Prasad, S., Bhalerao, A., & Cucullo, L. (2019). NRF2 and NF-κB interplay in cerebrovascular and neurodegenerative disorders: Molecular mechanisms and possible therapeutic approaches. *Redox Biology, 21*, 101059. https://doi.org/10.1016/j.redox.2018.11.017

Taylor, A. R., Gifondorwa, D. J., Robinson, M. B., Strupe, J. L., Prevette, D., Johnson, J. E., Hempstead, B., Oppenheim, R. W., & Milligan, C. E. (2012). Motoneuron programmed cell death in response to proBDNF. *Developmental Neurobiology, 72*(5), 699–712. https://doi.org/10.1002/dneu.20964

Vella, J., Zammit, C., Di Giovanni, G., Muscat, R., & Valentino, M. (2015). The central role of aquaporins in the pathophysiology of ischemic stroke. *Frontiers in Cellular Neuroscience, 9*, 108. https://doi.org/10.3389/fncel.2015.00108

Wang, P., Pan, R., Weaver, J., Jia, M., Yang, X., Yang, T., Liang, J., & Liu, K. J. (2021). MicroRNA-30a regulates acute cerebral ischemia-induced blood-brain barrier damage through ZnT4/zinc pathway. *Journal of Cerebral Blood Flow and Metabolism, 41*(3), 641–655. https://doi.org/10.1177/0271678X20926787

Wang, Z., Higashikawa, K., Yasui, H., Kuge, Y., Ohno, Y., Kihara, A., Midori, Y. A., Houkin, K., & Kawabori, M. (2020). FTY720 protects against ischemia-reperfusion injury by preventing the redistribution of tight junction proteins and decreases inflammation in the subacute phase in an experimental stroke model. *Translational Stroke Research, 11*(5), 1103–1116. https://doi.org/10.1007/s12975-020-00789-x

Williamson, M. R., Fuertes, C. J. A., Dunn, A. K., Drew, M. R., & Jones, T. A. (2021). Reactive astrocytes facilitate vascular repair and remodeling after stroke. *Cell Reports, 35*(4), 109048. https://doi.org/10.1016/j.celrep.2021.109048

Wu, L., Ye, Z., Pan, Y., Li, X., Fu, X., Zhang, B., Li, Y., Lin, W., Li, X., & Gao, Q. (2018). Vascular endothelial growth factor aggravates cerebral ischemia and reperfusion-induced blood-brain-barrier disruption through regulating LOC102640519/HOXC13/ZO-1 signaling. *Experimental Cell Research, 369*(2), 275–283. https://doi.org/10.1016/j.yexcr.2018.05.029

Wu, L., Zhao, K. Q., Wang, W., Cui, L. N., Hu, L. L., Jiang, X. X., Shuai, J., & Sun, Y. P. (2020). Nuclear receptor coactivator 6 promotes HTR-8/SVneo cell invasion and migration by activating NF-κB-mediated MMP9 transcription. *Cell Proliferation, 53*(9), e12876. https://doi.org/10.1111/cpr.12876

Xia, Y. P., He, Q. W., Li, Y. N., Chen, S. C., Huang, M., Wang, Y., Gao, Y., Huang, Y., Wang, M. D., Mao, L., & Hu, B. (2013). Recombinant human sonic hedgehog protein regulates the expression of ZO-1 and occludin by activating angiopoietin-1 in stroke damage. *PLoS One, 8*(7), e68891. https://doi.org/10.1371/journal.pone.0068891

Xu, F., Chen, L., Zhao, X., Zhong, H., Cui, L., Jiang, L., Huang, H., Li, L., Zeng, S., & Li, M. (2017). Interaction of Wip1 and NF-κB regulates neuroinflammatory response in astrocytes. *Inflammation Research, 66*(11), 1011–1019. https://doi.org/10.1007/s00011-017-1085-8

Yang, J., Vitery, M. D. C., Chen, J., Osei-Owusu, J., Chu, J., & Qiu, Z. (2019). Glutamate-releasing SWELL1 channel in astrocytes modulates synaptic transmission and promotes brain damage in stroke. *Neuron, 102*(4), 813–827.e816. https://doi.org/10.1016/j.neuron.2019.03.029

Yang, Y., Estrada, E. Y., Thompson, J. F., Liu, W., & Rosenberg, G. A. (2007). Matrix metalloproteinase-mediated disruption of tight junction proteins in cerebral vessels is reversed by synthetic matrix metalloproteinase inhibitor in focal ischemia in rat. *Journal of Cerebral Blood Flow and Metabolism, 27*(4), 697–709. https://doi.org/10.1038/sj.jcbfm.9600375

Yuan, W., Ibáñez, C. F., & Lin, Z. (2019). Death domain of p75 neurotrophin receptor: A structural perspective on an intracellular signalling

hub. *Biological Reviews of the Cambridge Philosophical Society*, *94*(4), 1282–1293. https://doi.org/10.1111/brv.12502

Zaghloul, N., Kurepa, D., Bader, M. Y., Nagy, N., & Ahmed, M. N. (2020). Prophylactic inhibition of NF-κB expression in microglia leads to attenuation of hypoxic ischemic injury of the immature brain. *Journal of Neuroinflammation*, *17*(1), 365. https://doi.org/10.1186/s12974-020-02031-9

Zhan, J., Qin, W., Zhang, Y., Jiang, J., Ma, H., Li, Q., & Luo, Y. (2016). Upregulation of neuronal zinc finger protein A20 expression is required for electroacupuncture to attenuate the cerebral inflammatory injury mediated by the nuclear factor-kB signaling pathway in cerebral ischemia/reperfusion rats. *Journal of Neuroinflammation*, *13*(1), 258. https://doi.org/10.1186/s12974-016-0731-3

Zhang, S., An, Q., Wang, T., Gao, S., & Zhou, G. (2018). Autophagy- and MMP-2/9-mediated reduction and redistribution of ZO-1 contribute to hyperglycemia-increased blood-brain barrier permeability during early reperfusion in stroke. *Neuroscience*, *377*, 126–137. https://doi.org/10.1016/j.neuroscience.2018.02.035

Zhang, X., Tang, X., Ma, F., Fan, Y., Sun, P., Zhu, T., Zhang, J., Hamblin, M. H., Chen, Y. E., & Yin, K. J. (2020). Endothelium-targeted overexpression of Krüppel-like factor 11 protects the blood-brain barrier function after ischemic brain injury. *Brain Pathology*, *30*(4), 746–765. https://doi.org/10.1111/bpa.12831

Zuo, G., Zhang, D., Mu, R., Shen, H., Li, X., Wang, Z., Li, H., & Chen, G. (2018). Resolvin D2 protects against cerebral ischemia/reperfusion injury in rats. *Molecular Brain*, *11*(1), 9. https://doi.org/10.1186/s13041-018-0351-1

SUPPORTING INFORMATION

Additional supporting information may be found in the online version of the article at the publisher's website.